



# **Modeling and Stability Analysis of Inverter-based Resources**

**Professor Lingling Fan, University of South Florida**

**May 8<sup>th</sup>, 2024, IEEE PES Live Webinars**

# Learning Objectives

- Discuss key points related to IBR generator interconnection reliability analysis
- Demonstrate dynamic phenomenon root cause analysis
- Explain converter control design for grid services & operation

## Fundamentals

EMT testbed building  
& experiment design

IBR converter control  
fundamentals:  
Grid-following & grid-forming  
design

Analysis: control performance &  
stability & parameter tuning

## Advanced techniques

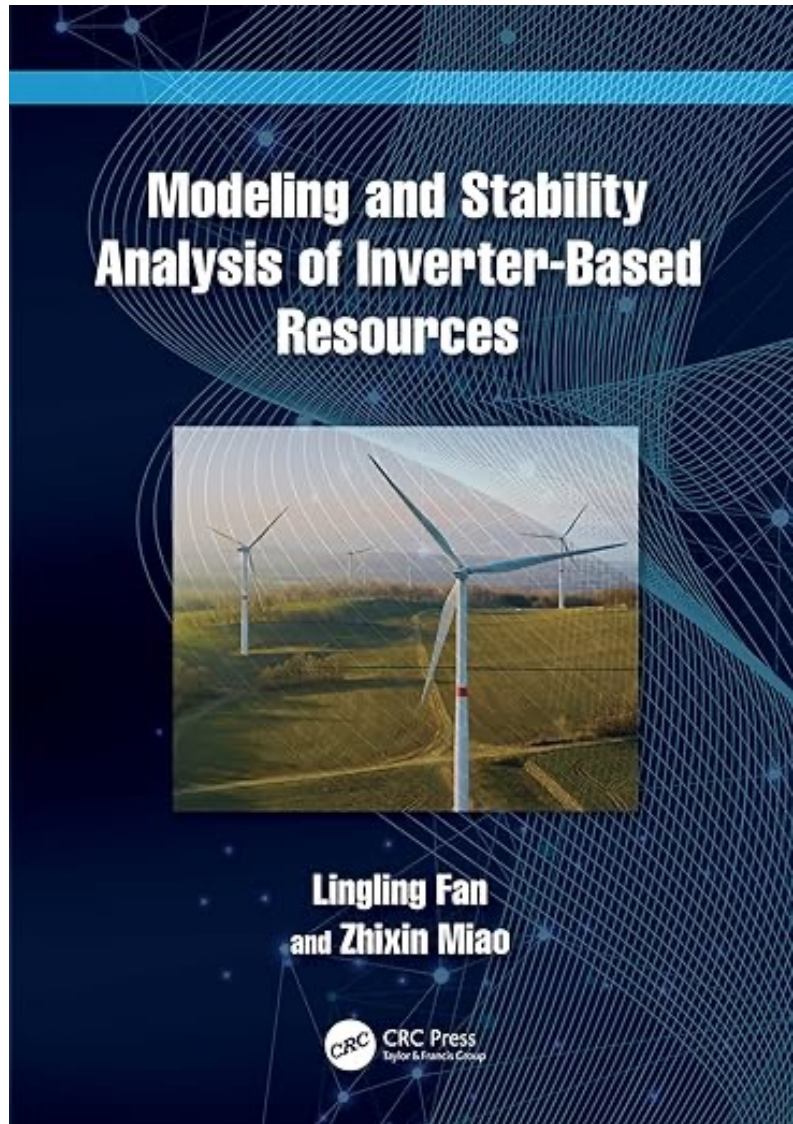
Analytical model  
building →  
Linear models, modal  
analysis

From data to  
models:  
Very useful (analysis,  
model reduction)

Frequency-domain  
analysis: MIMO, modal  
analysis, decomposition

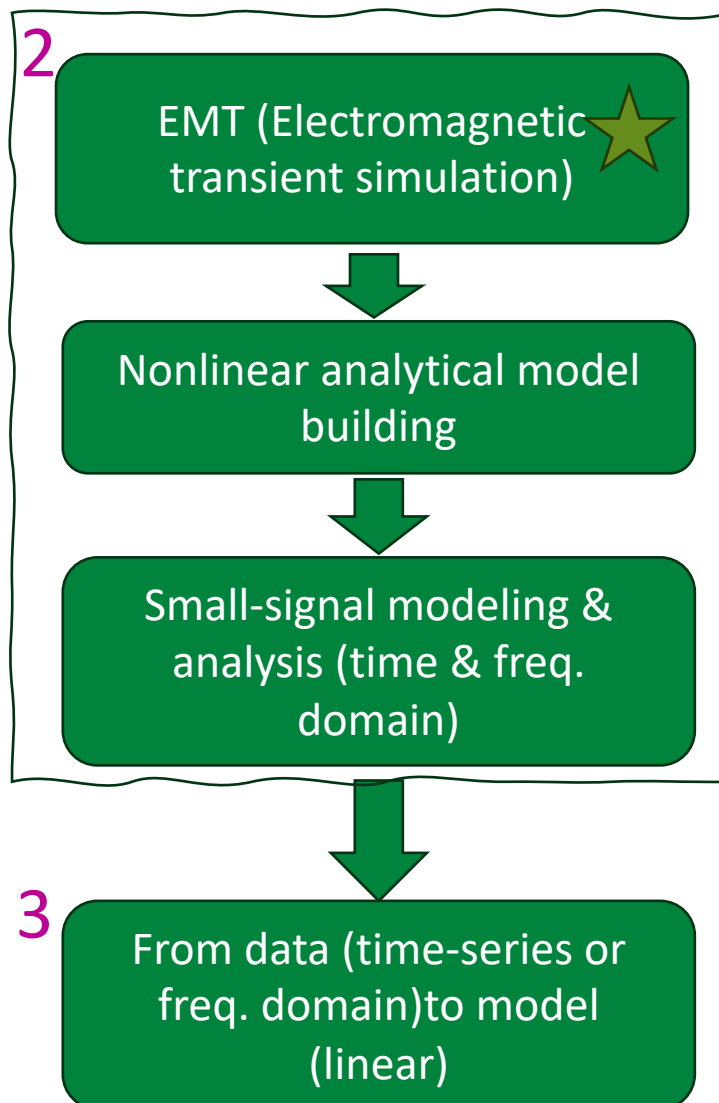
S-domain circuits:  
stability analysis for  
unbalanced & harmonic  
conditions

# Table of Contents



<b>Chapter 1</b>	Introduction .....	3
1.1	Why this book? .....	3
1.2	Book structure.....	4
1.3	Features and highlights .....	5
<b>Chapter 2</b>	Tools: simulation and analysis .....	7
2.1	Electromagnetic transient (EMT) simulation .....	7
2.1.1	Why to use an EMT package.....	8
2.1.2	How to master EMT.....	9
2.2	Per unit analysis.....	20
2.2.1	Per unit as scaling .....	22
2.2.2	Individual versus aggregated models .....	23
2.2.3	Equations with coefficients .....	24
2.2.4	System strength and short circuit ratio ( $SCR$ ) .....	25
2.3	Analytical dynamic model building.....	25
2.3.1	Frame conversion in space .....	25
2.3.2	Frame conversion between the time and frequency domains .....	26
2.3.3	A three-phase phase-locked loop (PLL) .....	26
2.3.4	A single-phase PLL.....	27
2.3.5	An RLC circuit.....	31
2.4	Small-signal analysis .....	34
2.4.1	Modal analysis .....	35
2.4.2	Block diagram and frequency-domain analysis .....	36
2.4.3	Interactions of two RLC branches in a circuit .....	36
2.5	Summary.....	42
<b>Chapter 3</b>	Tools: measurement-based modeling .....	44
3.1	A tutorial example .....	45
3.2	Model development .....	50
3.2.1	Modeling the dc side dynamics of a solar PV.....	51
3.2.2	Modeling PLLs with sophisticated structures.....	53
3.3	Frequency scan: $dq$ admittance .....	61
3.3.1	Admittance measurement based on frequency scans.....	62
3.4	Frequency scan: sequence-domain admittance.....	63
3.4.1	Injection frequency above the fundamental frequency .....	63
3.4.2	Injection frequency at the mirror frequency .....	65

<p><b>Part II Inverter-Based Resources: Detailed Examination</b></p> <p><b>Chapter 4</b> Control of IBR power plants ..... 73</p> <ul style="list-style-type: none"> <li>4.1 Grid-following control ..... 73           <ul style="list-style-type: none"> <li>4.1.1 The actuator: the converter voltage ..... 73</li> <li>4.1.2 More about frame conversion ..... 76</li> <li>4.1.3 Outer control design ..... 79</li> <li>4.1.4 Inner current control ..... 87</li> <li>4.1.5 PLL design ..... 94</li> <li>4.1.6 EMT simulation results ..... 96</li> </ul> </li> <li>4.2 Plant-level control ..... 98           <ul style="list-style-type: none"> <li>4.2.1 Bandwidth of IBR contr. ..... 100</li> <li>4.2.2 EMT simulation results ..... 102</li> </ul> </li> <li>4.3 Synchronization techniques ..... 103</li> <li>4.4 Summary ..... 105</li> </ul> <p><b>Chapter 5</b> Analytical modeling of a GFL-IBR ..... 106</p> <ul style="list-style-type: none"> <li>5.1 A simplified linear model ..... 106           <ul style="list-style-type: none"> <li>5.1.1 Application: weak grid voltage instability mechanism ..... 108</li> </ul> </li> <li>5.2 Analysis of real-world 0.1-Hz oscillation event ..... 113</li> <li>5.3 Current source-based model with PLL included ..... 117           <ul style="list-style-type: none"> <li>5.3.1 A second-order model ..... 118</li> <li>5.3.2 PLL and negative impedance ..... 119</li> <li>5.3.3 A linearized model ..... 121</li> </ul> </li> <li>5.4 PLL weak grid stability: inclusion of grid dynamics ..... 127</li> <li>5.5 Nonlinear analytical models of a GFL-IBR ..... 134           <ul style="list-style-type: none"> <li>5.5.1 The testbed ..... 134</li> <li>5.5.2 State-space representation ..... 135</li> </ul> </li> <li>5.6 Applications of the nonlinear analytical models ..... 138           <ul style="list-style-type: none"> <li>5.6.1 Parameterization of a simplified model ..... 138</li> <li>5.6.2 Weak grid oscillation analysis ..... 140</li> <li>5.6.3 Interactions of PLL and the rest of the system ..... 151</li> </ul> </li> <li>5.7 GFL with static-frame current control ..... 156           <ul style="list-style-type: none"> <li>5.7.1 The study system and the key challenges ..... 156</li> <li>5.7.2 Comparison of the analytical model and the EMT model ..... 159</li> <li>5.7.3 Applications of the analytical model ..... 159</li> <li>5.7.4 Analysis of a real-world 20-Hz oscillation event ..... 161</li> </ul> </li> <li>5.8 Summary ..... 166</li> </ul> <p><b>Chapter 6</b> Grid-forming (GFM) control ..... 168</p> <ul style="list-style-type: none"> <li>6.1 Multi-loop GFM: from GFL to GFM ..... 170</li> <li>6.2 GFM1: advanced GFL ..... 170</li> <li>6.3 GFM2: the conventional design ..... 171</li> </ul>	<p>Go to page 206</p> <p><b>Chapter 7</b> Type-3 wind farms ..... 179</p> <ul style="list-style-type: none"> <li>6.4 GFM3: minimal edits ..... 174</li> <li>6.5 Virtual synchronous machines (VSM) ..... 176</li> <li>6.6 Summary ..... 177</li> </ul> <p><b>Chapter 8</b> Power networks with multiple IBRs ..... 203</p> <ul style="list-style-type: none"> <li>7.1 Analysis of induction generator effect (IGE) ..... 179           <ul style="list-style-type: none"> <li>7.1.1 Example 1: subsynchronous resonance due to induction generator effect ..... 181</li> </ul> </li> <li>7.2 An EMT test case of SSR ..... 183</li> <li>7.3 Analytical modeling ..... 187           <ul style="list-style-type: none"> <li>7.3.1 <math>dq</math>-frame dynamic models ..... 189</li> <li>7.3.2 Steady-state computation ..... 193</li> <li>7.3.3 Simscape SPS implementation ..... 198</li> <li>7.3.4 Applications ..... 200</li> </ul> </li> <li>7.4 Summary ..... 202</li> </ul> <p><b>Part III Generalized Dynamic Circuits</b></p> <p><b>Chapter 9</b> Generalized dynamic circuits ..... 231</p> <ul style="list-style-type: none"> <li>8.1 Inter-IBR oscillation mode ..... 203           <ul style="list-style-type: none"> <li>8.1.1 Block diagram construction and integration techniques ..... 203</li> <li>8.1.2 Simulation results ..... 206</li> <li>8.1.3 Modal analysis ..... 206</li> <li>8.1.4 Two decoupled circuits ..... 209</li> </ul> </li> <li>8.2 A three-generator power grid ..... 211           <ul style="list-style-type: none"> <li>8.2.1 Nonlinear analytical modeling ..... 211</li> <li>8.2.2 Admittance-based modeling ..... 218</li> </ul> </li> <li>8.3 Frequency-domain modal analysis ..... 223           <ul style="list-style-type: none"> <li>8.3.1 Admittance-based stability analysis ..... 223</li> <li>8.3.2 Basic mode shape analysis ..... 224</li> <li>8.3.3 Extended mode shape analysis ..... 226</li> </ul> </li> <li>8.4 Summary ..... 228</li> </ul>
--	---



- 4 Grid-following control design, implementation In EMT testbeds
- 5 Analytical model building: single-IBR infinite-bus testbeds
- 6 Grid-forming control design & EMT testbeds
- 7 Type-3 wind farm: analytical model building & analysis
- 8 Multi-IBR systems: analytical model building & analysis

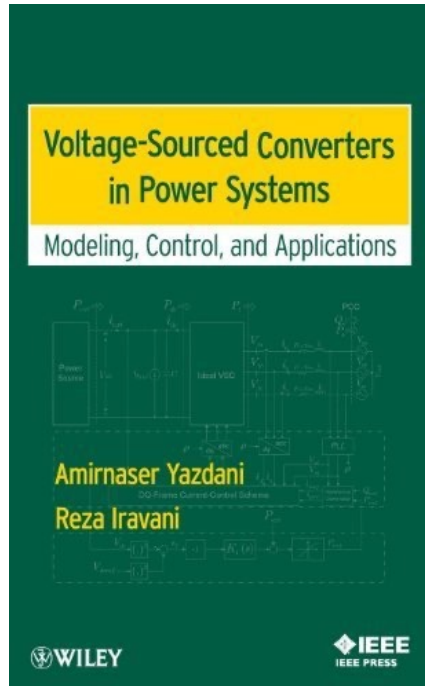
- 9 From steady-state circuits to generalized dynamic circuits  
→ stability/harmonic analysis
- Induction machines
  - Single-line ground faults
  - Synchronous generators
  - IBR: two-port circuits

# 1

Introduction:  
Highlights &

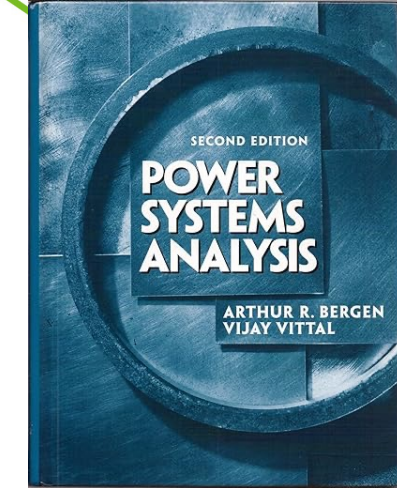
Comparison with the green book  
& Kundur's book

1. Numbers: easy to remember through **per-unit system**
2. **Insights revealing:** Frequency-domain analysis
3. Replicability: **Github codes & models**
4. Up to date coverage: **GFL vs GFM**
5. **Advanced tech:** system identification; s-domain circuits

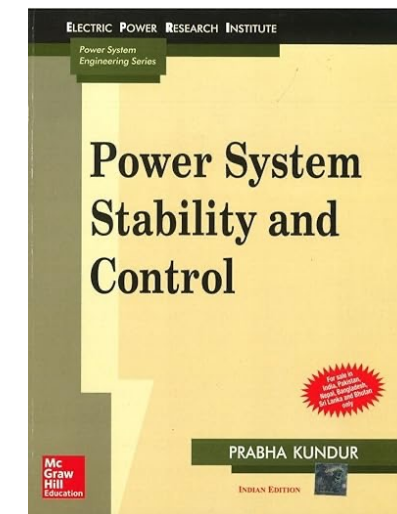


Physical unit based  
**Bode diagram-based analysis**

Domain:  
Grid-following control (GFL)  
Fixed-frequency control



**Root Locus diagram**



Per unit based  
State-space modeling  
**Eigenvalue-based analysis**  
Domain: conventional power grid

# Highlights

- **Critical concept explained:** a very easy guide on frame conversion
  - Static/dq, Park: abc to dq, Clarke: abc to  $\alpha\beta$
- **Number matters**
  - Per unit-based converter control design
- **Github codes & models**
- **Design & analysis:**
  - Form feedback systems
- **s-domain circuits:**
  - revisit & generalize a few popular circuits

# Critical concept explained:

Frame conversion in the space

# Frame conversion in space: chapters 2

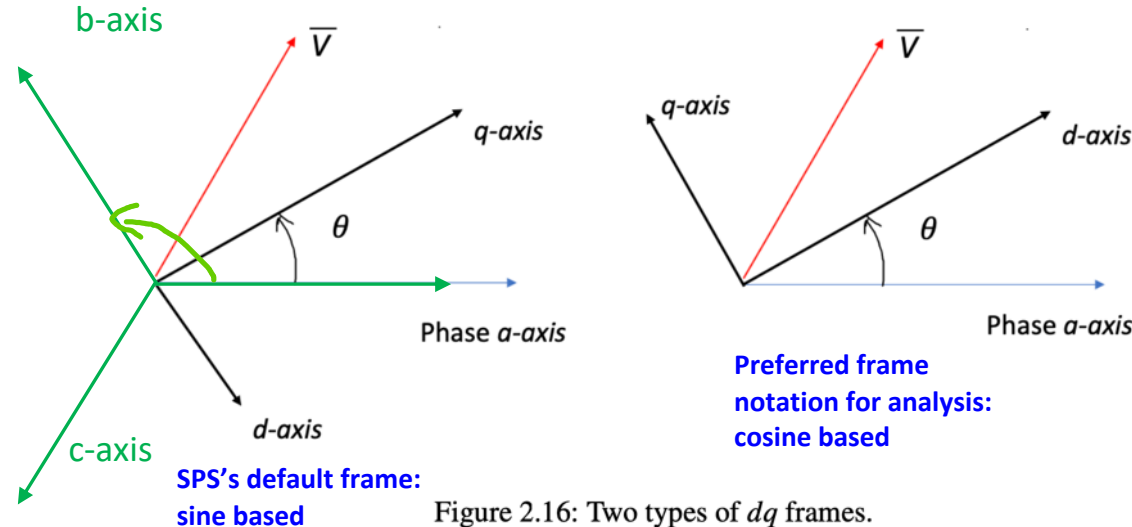


Figure 2.16: Two types of *dq* frames.

## Frame 1: dq to abc

$$\begin{bmatrix} v_a \\ v_b \\ v_c \end{bmatrix} = \begin{bmatrix} \sin \theta & \cos \theta & 1 \\ \sin(\theta - \frac{2\pi}{3}) & \cos(\theta - \frac{2\pi}{3}) & 1 \\ \sin(\theta + \frac{2\pi}{3}) & \cos(\theta + \frac{2\pi}{3}) & 1 \end{bmatrix} \begin{bmatrix} v_d \\ v_q \\ v_0 \end{bmatrix} \quad (2.8)$$

**abc to dq:** inverse of the above matrix

$$\begin{bmatrix} v_d \\ v_q \\ v_0 \end{bmatrix} = \frac{2}{3} \begin{bmatrix} \sin \theta & \sin(\theta - \frac{2\pi}{3}) & \sin(\theta + \frac{2\pi}{3}) \\ \cos \theta & \cos(\theta - \frac{2\pi}{3}) & \cos(\theta + \frac{2\pi}{3}) \\ \frac{1}{2} & \frac{1}{2} & \frac{1}{2} \end{bmatrix} \begin{bmatrix} v_a \\ v_b \\ v_c \end{bmatrix} \quad (2.9)$$

**Recommend to use complex vectors and geometry for frame conversion**

## Frame 1:

$$v_a = \Re \{(v_d + jv_a)e^{j(\theta - \frac{\pi}{2})}\} = \Re \{(v_q - jv_d)e^{j\theta}\}$$

$$v_b = \Re \{(v_q - jv_d)e^{j(\theta - \frac{2\pi}{3})}\}$$

$$v_c = \Re \{(v_q - jv_d)e^{j(\theta + \frac{2\pi}{3})}\}$$

## Frame 2: abc to space vector to the dq

$$\begin{aligned} \bar{V} &= \vec{v} e^{-j\theta} = \frac{2}{3} (v_a + e^{j\frac{2\pi}{3}} v_b + e^{-j\frac{2\pi}{3}} v_c) e^{-j\theta} \\ &= \frac{2}{3} \begin{bmatrix} e^{-j\theta} & e^{-j(\theta - \frac{2\pi}{3})} & e^{-j(\theta + \frac{2\pi}{3})} \end{bmatrix} \begin{bmatrix} v_a \\ v_b \\ v_c \end{bmatrix} \end{aligned} \quad (2.14)$$

Separating the real and imaginary parts, we get again the vector/matrix format:

$$\begin{bmatrix} v_d \\ v_q \\ v_0 \end{bmatrix} = \frac{2}{3} \begin{bmatrix} \cos \theta & \cos(\theta - \frac{2\pi}{3}) & \cos(\theta + \frac{2\pi}{3}) \\ -\sin \theta & -\sin(\theta - \frac{2\pi}{3}) & -\sin(\theta + \frac{2\pi}{3}) \end{bmatrix} \begin{bmatrix} v_a \\ v_b \\ v_c \end{bmatrix} \quad (2.15)$$

## More on frame conversion in space: chapter 4.1.2

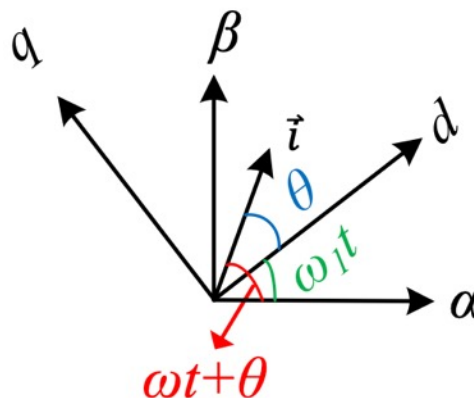


Figure 4.3: The  $\alpha\beta$  frame and the  $dq$  frame.

$$i_a = \hat{i} \cos(\omega t + \theta) \quad (4.17a)$$

$$i_b = \hat{i} \cos \left( \omega t + \theta - \frac{2\pi}{3} \right) \quad (4.17b)$$

$$i_c = \hat{i} \cos \left( \omega t + \theta + \frac{2\pi}{3} \right) \quad (4.17c)$$

$$\vec{i} = \frac{2}{3} (i_a + a i_b + a^2 i_c) = i_\alpha + j i_\beta \quad (4.19)$$

Clarke transformation

$$\begin{bmatrix} i_\alpha \\ i_\beta \end{bmatrix} = \frac{2}{3} \begin{bmatrix} 1 & \cos(\frac{2\pi}{3}) & \cos(-\frac{2\pi}{3}) \\ 0 & \sin(\frac{2\pi}{3}) & \sin(-\frac{2\pi}{3}) \end{bmatrix} \begin{bmatrix} i_a \\ i_b \\ i_c \end{bmatrix}$$

$$\begin{bmatrix} i_\alpha \\ i_\beta \end{bmatrix} = \frac{2}{3} \begin{bmatrix} 1 & -\frac{1}{2} & -\frac{1}{2} \\ 0 & \frac{\sqrt{3}}{2} & -\frac{\sqrt{3}}{2} \end{bmatrix} \begin{bmatrix} i_a \\ i_b \\ i_c \end{bmatrix}$$

Park transformation

$$\begin{aligned} \bar{I}_{dq} &= \vec{i} e^{-j\theta_{dq}} \\ &= \frac{2}{3} (i_a + a i_b + a^2 i_c) e^{-j\theta_{dq}} \\ &= \frac{2}{3} (i_a e^{-j\theta_{dq}} + e^{-j(\theta_{dq} - \frac{2\pi}{3})} i_b + e^{-j(\theta_{dq} + \frac{2\pi}{3})} i_c). \end{aligned} \quad (4.23)$$

We can note  $\omega_1 t$  as  $\theta_{dq}$ .

- static frame:  $\vec{i} = \hat{i} e^{j(\omega t + \theta)}$ .

- dq frame:  $\bar{I}_{dq} = \vec{i} e^{-j\omega_1 t}$

$$\begin{bmatrix} i_d \\ i_q \end{bmatrix} = \begin{bmatrix} \cos \theta_{dq} & \cos(\theta_{dq} - \frac{2\pi}{3}) & \cos(\theta_{dq} + \frac{2\pi}{3}) \\ -\sin \theta_{dq} & -\sin(\theta_{dq} - \frac{2\pi}{3}) & -\sin(\theta_{dq} + \frac{2\pi}{3}) \end{bmatrix} \begin{bmatrix} i_a \\ i_b \\ i_c \end{bmatrix} \quad (4.24)$$

# Explanation of PLL (sensor of angle) using geometry

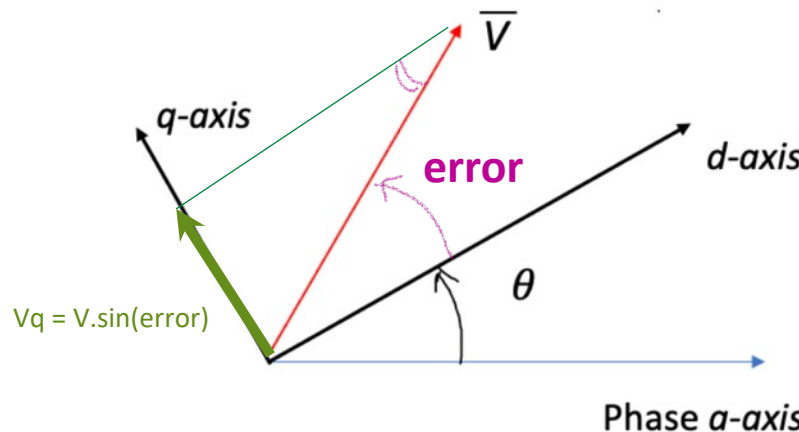


Fig. 2.16

- To track the voltage space vector's angle, **the d-axis will try to align with the vector.**
- This means that the **vector's projection to the q-axis** should be zero.
- PLL's function: to **enforce  $V_q = 0$**  by use of abc/dq conversion and further applying integral control.
- Since angle is a **ramp signal**, at least two **integral control** is required. The PLL in the previous page meets the requirement.

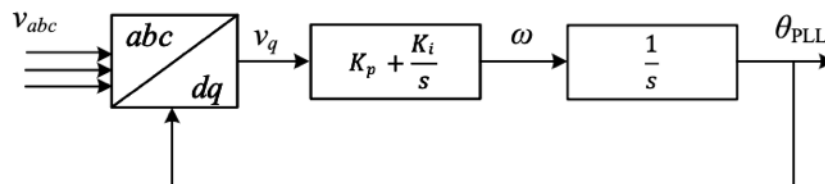


Figure 4.18: SRF-PLL.

# Number matters:

per unit-based design & analysis

# Per unit-based numerical systems: power electronics vs. power systems

IEEE TRANSACTIONS ON ENERGY CONVERSION, VOL. 32, NO. 3, SEPTEMBER 2017

1139

## Impedance Modeling of Three-Phase Voltage Source Converters in DQ, Sequence, and Phasor Domains

Shahil Shah, Student Member, IEEE, and Leila Parsa, Senior Member, IEEE

**Abstract**—This paper presents a modular approach for the impedance modeling of three-phase voltage source converters (VSC) by representing the VSC dynamics using three-by-three transfer matrix in the sequence, phasor, and DQ domains. The transfer matrix based impedance modeling process by sequence modeling the ac and dc side dynamics, and describing the VSC dynamics independent of the ac and dc side networks. It also explicitly captures coupling among the dominant frequency components of the ac and dc side voltages and currents in the off-diagonal elements. Modeling of the VSC ac and dc side impedances, including the effects of the network on the other side of the VSC, is presented using the transfer matrix models. Transfer matrix based impedance modeling of the ac and dc side networks and stability analysis case studies are presented for a VSC-based HVDC station in an offshore wind farm. It is shown that the coupling between the ac and dc networks, and between the positive and negative sequence components of the three-phase quantities, play an important role in the low-frequency stability of the VSC. Impedance models and stability analysis predictions are validated using the wind farm simulations.

**Index Terms**—Stability, offshore wind farm, impedance modeling, HVDC transmission, voltage source converters, resonance.

### I. INTRODUCTION

THREE-PHASE voltage source converters (VSC) are basic building blocks of many power electronic equipments in offshore wind farms such as wind turbines, HVDC stations, and STATCOM units. Unstable interaction between these VSCs and networks at their terminals is a potential threat to the operation of the entire farm [1]. Impedance-based stability analysis is an attractive tool for the evaluation of such interactions [2].

Models for the ac-side impedance of VSC are developed in the dq domain [3], [4], and more recently in the sequence domain [5]. Both the dq and sequence domain modeling have ignored the effects of the network at the dc terminals, by representing it either by a constant power load [3] or a voltage source [4], [5]. Similarly, dc-side impedance modeling has ignored the ac network dynamics [6], [7]. Coupling between the ac and dc networks through a VSC, however, may have a critical influence on the VSC stability and cannot always be ignored [8].

Manuscript received September 8, 2016; revised December 12, 2016 and March 5, 2017; accepted April 14, 2017. Date of publication April 26, 2017; date of current version August 18, 2017. Paper no. TEC-00772-2016. (Corresponding Author: Shahil Shah.)

The authors are with the Department of Electrical, Computer and Systems Engineering, Rensselaer Polytechnic Institute, Troy, NY 12180 USA (e-mail: shahil12@rpi.edu; parsal@ececs.rpi.edu).

Color versions of one or more of the figures in this paper are available online at <http://ieeexplore.ieee.org>.

Digital Object Identifier 10.1109/TEC.2017.2698202

0885-8969 © 2017 IEEE. Personal use is permitted, but republication/redistribution requires IEEE permission. See [http://www.ieee.org/publications\\_standards/publications/rights/index.html](http://www.ieee.org/publications_standards/publications/rights/index.html) for more information.

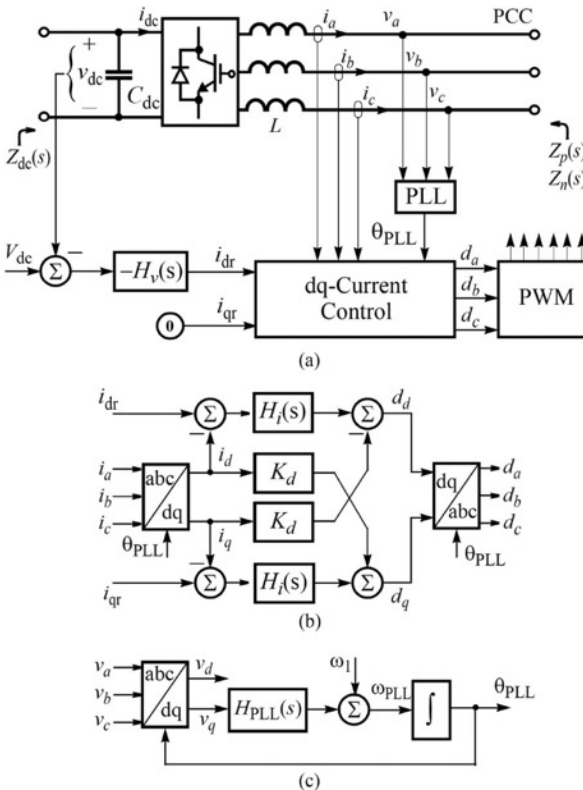


Fig. 2. Grid-connected VSC in offshore wind farm with VSC-HVDC transmission to grid. a) Onshore VSC-HVDC station with dc bus voltage control, b) dq-domain ac current control, and c) PLL.

- Difficult to relate the PLL parameters with bandwidth.
- Also to achieve the same bandwidth, PLL parameters change significantly for different voltage levels.

TABLE I  
PARAMETERS FOR SIMULATION

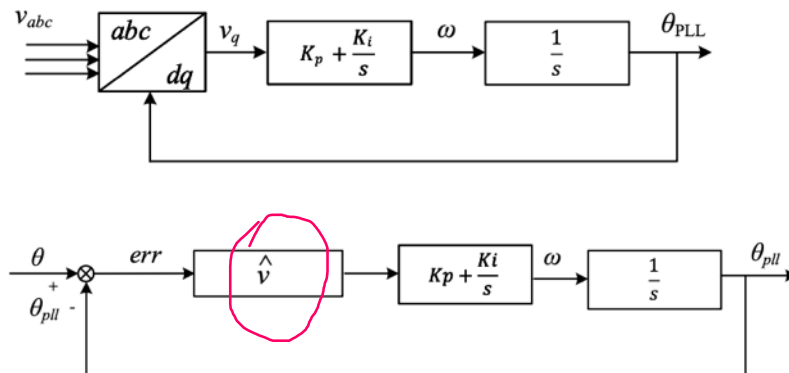
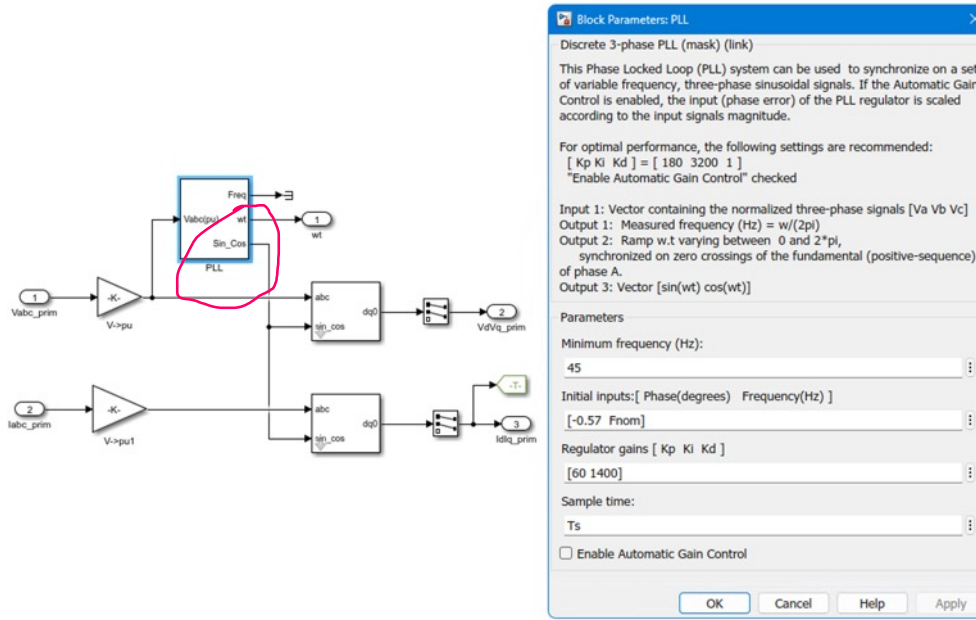
Parameter	Value
Wind farm power output, $P_0$	30 MW
PCC current (peak), $I_1$	1.63 kA
PCC voltage (peak), $V_1$	12.25 kV
DC-bus voltage, $V_{dc}$	30.0 kV
Current compensator, $H_i(s)$	$(5 + 75.4/s)/30 \times 10^3$
PLL compensator, $H_{PLL}(s)$	$0.01 + 2.051/s$
DC-bus voltage compensator, $H_v(s)$	$0.01 + 1.215/s$
Decoupling gain, $k_d$	1.5
Phase reactor, $L$	4.0 mH
DC-link capacitor, $C_{dc}$	$67.7 \mu F$
Short-circuit ratio, SCR	2.5
Grid inductance, $L_g$	7.8 mH
Grid resistance, $R_g$	0.52 Ω
Filter inductor, $L_f$	0.18 mH
Filter capacitor, $C_f$	$35.0 \mu F$
Damping resistor, $R_d$	2.3 Ω
HVDC cable inductance, $L_{cab}$	2.0 mH
Equivalent capacitance of wind farm, $C_{eq}$	0.72 mF

$$H_{PLL}(s) = 0.018 + 5.7/s \quad (51)$$

50 Hz bandwidth

30 Hz  
bandwidth

# PLL parameters used in MATLAB/Simscape Specialized power systems (SPS)



$$\frac{\theta_{\text{PLL}}}{\theta} = \frac{\left(K_p + \frac{K_i}{s}\right) \frac{1}{s}}{1 + \left(K_p + \frac{K_i}{s}\right) \frac{1}{s}} = \frac{K_p s + K_i}{s^2 + K_p s + K_i}$$

```

Kp = 20; Ki = 200; G_open = (Kp+Ki/s)/s;
G1 = feedback(G_open, 1);
Kp = 60; Ki = 1400; G_open = (Kp+Ki/s)/s;
G2 = feedback(G_open, 1);
Kp = 150; Ki = 3200; G_open = (Kp+Ki/s)/s;
G3 = feedback(G_open, 1);
figure;
bode(G1,'b', G2, 'r', G3, 'k'); grid on;
legend('(20,200)', '(60, 1400)', '(150, 3200)');
xlim([1, 1000]);
figure; step(G1,'b', G2,'r', G3,'k'); grid on

```

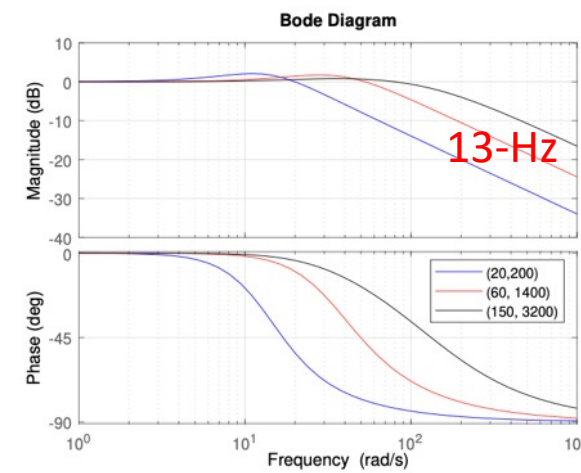


Figure 4.20: PLL closed-loop systems: frequency responses

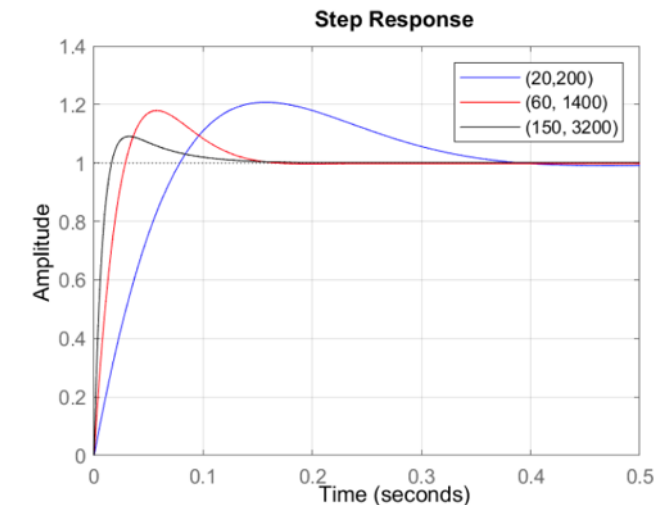


Figure 4.21: PLL closed-loop systems: step responses.

5-Hz

13 Hz

27 Hz

# Benefits of per unit-based numerical values

Easy to **remember** the typical numbers: PLL: (60, 1400)

Easy to **relate** numbers with performance: PLL (60, 1400) => 13 Hz

Other examples:

- Choke filter parameters:  $X = 0.15 \text{ pu}$ ;  $R = 0.03 \text{ pu}$ ; same for a 1-MW converter and a 100-MW IBR (100 1-MW inverters in parallel)
- DC-link capacitor parameters: time constant is 0.0272 seconds. Same for a 2-MW turbine or a 200-MW equivalent turbine.

$$V_{\text{dc}} C_{\text{dc}} \frac{dV_{\text{dc}}}{dt} = P_{\text{dc}} - P_{\text{ac}} \quad (4.34)$$

$$\frac{1}{2} \cdot C_{\text{dc}} \frac{dV_{\text{dc}}^2}{dt} = P_{\text{dc}} - P_{\text{ac}}. \quad (4.35)$$

$$\frac{\frac{1}{2} C_{\text{dc}} V_{\text{dc},\text{base}}^2}{P_b} \frac{d(V_{\text{dc}}^{\text{pu}})^2}{dt} = P_{\text{dc}}^{\text{pu}} - P_{\text{ac}}^{\text{pu}}. \quad (4.36)$$

$$\tau_{\text{dc}} \frac{dV_{\text{dc}}^2}{dt} = P_{\text{dc}} - P = P_{\text{dc}} - Vi_d^*. \quad (4.37)$$

**Table 4.1**  
**Data of Simscape power system examples**

Device	ac voltage	dc voltage	dc-link capacitor
1.5-MW DFIG	575 V	1150 V	0.01 F
2-MW type-4	575 V	1100 V	0.09 F
100-kW PV inverter	260 V	500 V	0.06 F
250-kW PV inverter	250 V	480 V	0.0272 F
400-kW PV inverter	260 V	500 V	0.05 F

# Per-unit based converter control design: chapter 4

$$S^{\text{pu}} = \bar{V}^{\text{pu}} (\bar{I}^{\text{pu}})^*.$$

## Outer control design stage assumptions:

- In pu unit system
- inner control is very fast: current order = measurements
- Dq-frame is aligned with the PCC bus voltage space vector (PLL in place)

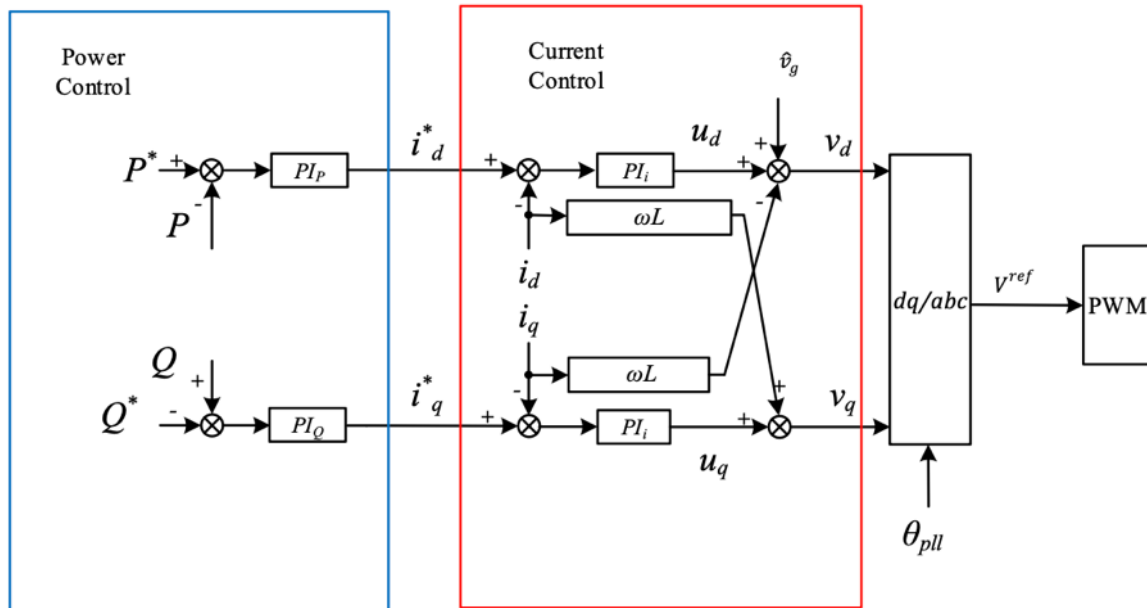


Figure 4.12: Inverter control.

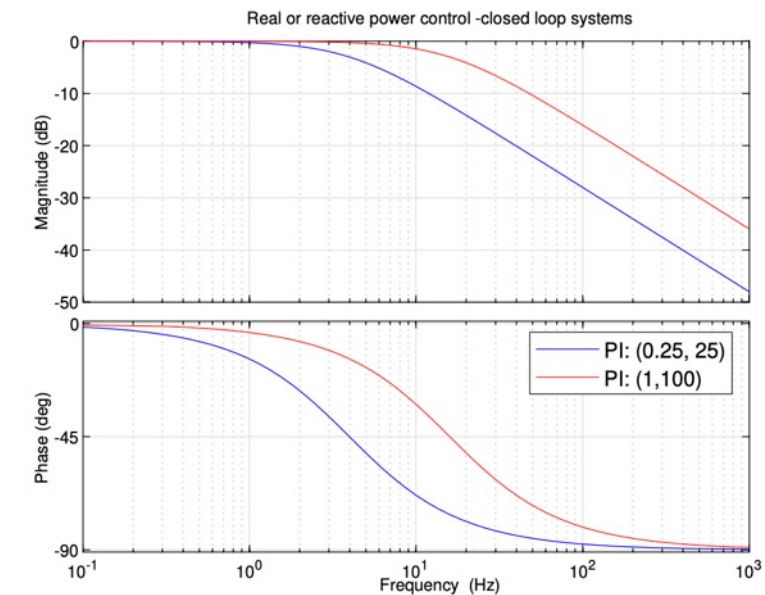
$$P = \hat{v}_g i_d \approx \hat{v}_g i_d^* \implies \frac{P}{i_d^*} = \hat{v}_g$$

$$Q = -\hat{v}_g i_q \approx -\hat{v}_g i_q^* \implies \frac{Q}{i_q^*} = -\hat{v}_g$$

$$\frac{P}{P^*} = \frac{K_p + \frac{K_i}{s}}{1 + K_p + \frac{K_i}{s}} = \frac{1 + s \frac{K_p}{K_i}}{1 + s \frac{1+K_p}{K_i}}$$

$$\frac{Q}{Q^*} = \frac{K_p + \frac{K_i}{s}}{1 + K_p + \frac{K_i}{s}} = \frac{1 + s \frac{K_p}{K_i}}{1 + s \frac{1+K_p}{K_i}}$$

PI parameters (0.25, 25)  $\rightarrow$  5-Hz bandwidth; 4-Hz if considering current tracking dynamics as  $1/(1+0.01s)$ .  
 (1, 100)  $\rightarrow$  16 Hz



# Per-unit based converter control design: chapter 4

## Inner control design stage assumptions:

- Outer control is very slow. Current orders are constant
- Cross coupling & feedforward in place

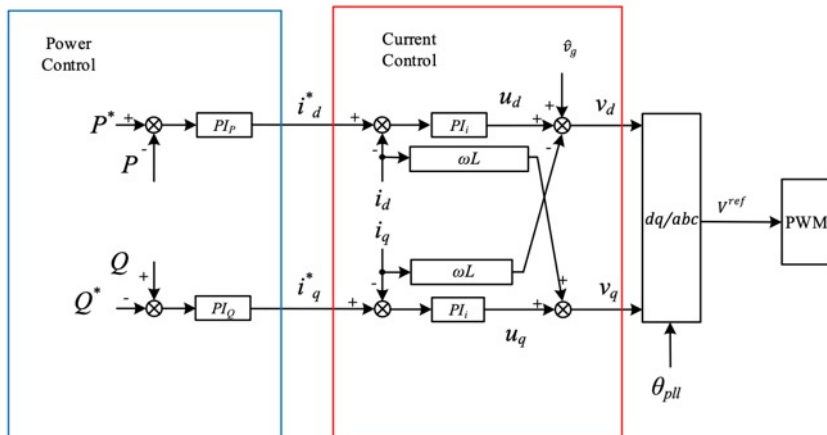


Figure 4.12: Inverter control.

$$L \frac{d\vec{i}_a}{dt} + R\vec{i}_a = \vec{v}_a - \vec{v}_{ga}$$

$$(R + j\omega L)\bar{I}_{dq} + L \frac{d\bar{I}_{dq}}{dt} = \bar{V}_{dq} - \bar{V}_{g,dq}$$

$$(R + (s + j\omega)L)\bar{I}_{dq} = \bar{V}_{dq} - \bar{V}_{g,dq}$$

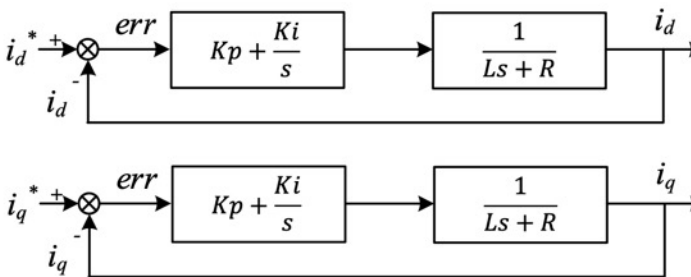


Figure 4.11: Current control design.

What is the plant model if  $R = 0.01 \text{ pu}$ ;  $X = 0.15 \text{ pu}$ ?

$$\frac{1}{0.01 + \frac{0.15}{377}s}.$$

$$\frac{R + sL}{Z_{\text{base}}} = \frac{R}{Z_{\text{base}}} + \frac{sL}{\omega_0 L_{\text{base}}} = R^{\text{pu}} + s \frac{L^{\text{pu}}}{\omega_0} = 0.01 + 3.98 \times 10^{-4} s.$$

```

G1 = feedback((Kp+Ki/s)*plant, 1);
G2 = feedback((0.4+3/s)*plant, 1);
G3 = feedback((1+3/s)*plant, 1);
G4 = feedback((1+0.03/s)*plant, 1);
[bandwidth(G1), bandwidth(G2), ...
bandwidth(G3), bandwidth(G4)]/2/pi

```

```

ans = 1x4
149.6443 147.9133 387.1436 386.6546

```

```

figure;
bode(G1,'b', G2,'r', G3,'g', G4,'k', bode_P); grid on;
xlim([10,500]);
legend('PI: (0.375, 28)', 'PI: (0.4, 3)', 'PI:(1,3)', 'PI:(1, 0.03)')

```

Typical parameters: (0.4, 3) → 150 Hz, (1, 3) → 400 Hz

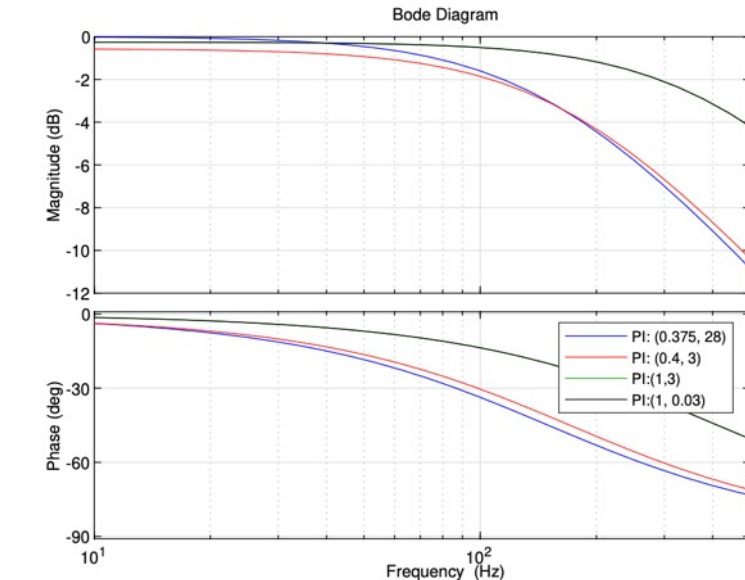


Figure 4.13: Inner current control performance check: frequency responses

Remarks on current controller:

- Ki's influence is insignificant, since at > 100 Hz range,  $1/(R+Ls)$  is equivalent to  $1/(Ls)$ .
- Tracking performance is influenced mainly by the proportional gain: Kp
- This fact aligns with the findings in the literature that inner current controller's Kp needs to be coordinated with PLL, e.g., [1]

[1] H. Gong, X. Wang and L. Harnefors, "Rethinking Current Controller Design for PLL-Synchronized VSCs in Weak Grids," in *IEEE Transactions on Power Electronics*, vol. 37, no. 2, pp. 1369-1381, Feb. 2022, doi: 10.1109/TPEL.2021.3105549.

# EMT testbeds available at Github

<https://github.com/fllseu/book-modeling-and-stability-analysis-of-IBRs>

Code

Issues

Pull requests

Actions

Projects

Security

Insights

## Files

main



Go to file

chapter2

analytical

PLL\_3phase.slx

PLL\_single.slx

example2\_3Leg2Level\_VSC.slx

example3\_VSC.slx

readme.md

single\_phasePLL\_stability.m

chapter6

GFM\_initial.m

README.md

testbed\_overall.slx

README.md

book-modeling-and-stability-analysis-of-IBRs / chapter2 / analytical /



fllseu

Update README.md

485995f · 4 months ago

History

Name	Last commit message	Last commit date
...		
README.md	Update README.md	4 months ago
init_sim_RLC.m	Add files via upload	4 months ago
sim_RLC.slx	Add files via upload	4 months ago
twoRLC_code_Fig2_27.mlx	Add files via upload	4 months ago
twoRLC_code_Fig2_27.pdf	Add files via upload	4 months ago

README.md



## Chapter 2

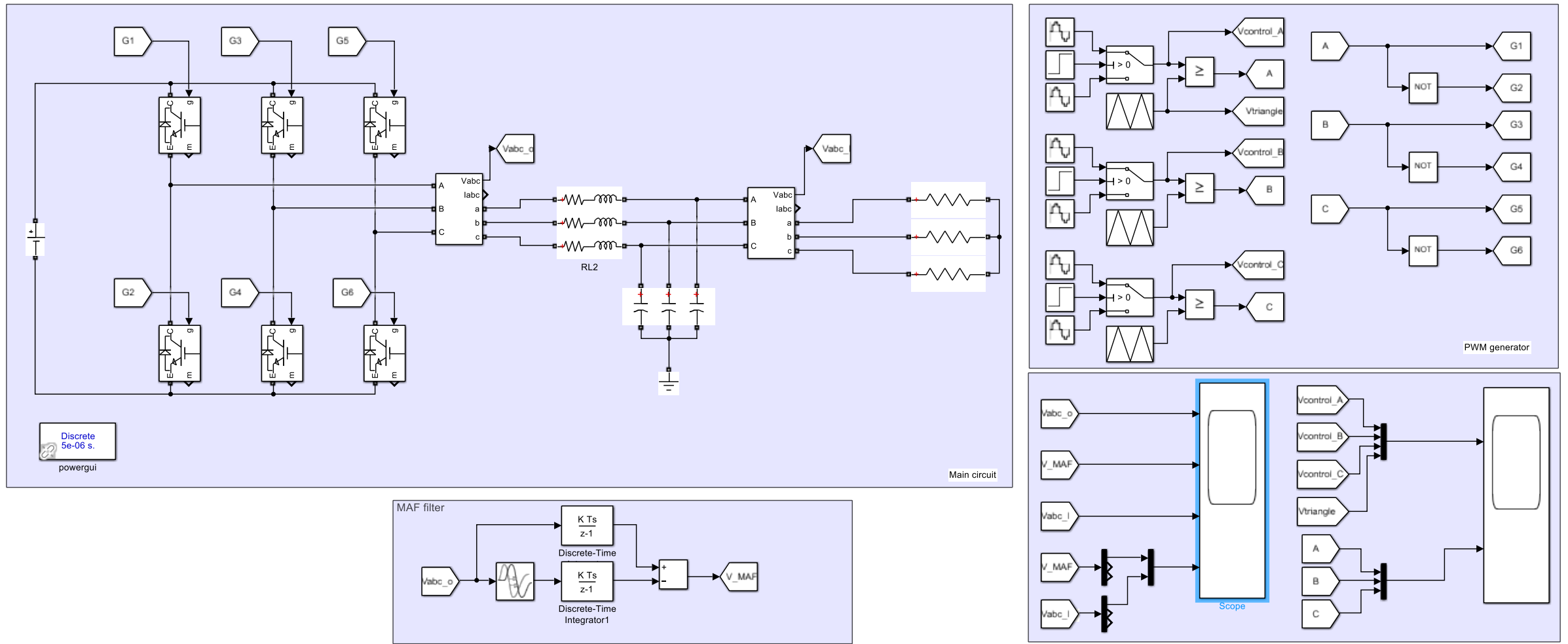
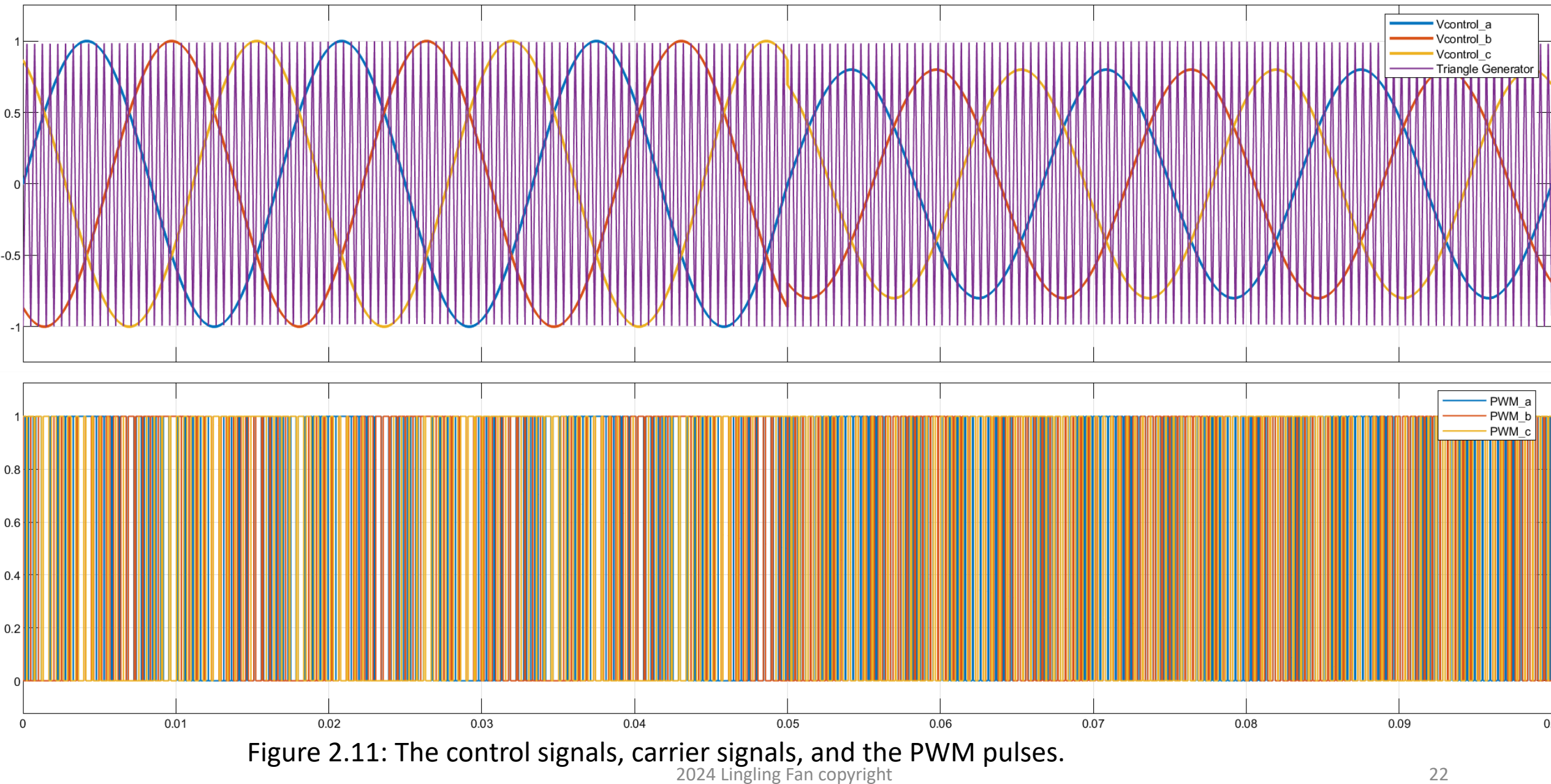


Figure 2.10 A three-phase two-level voltage source converter. The choke filter parameters:  $R = 0.02 \Omega$ ,  $L = 0.003 \text{ H}$ , the shunt capacitor  $C = 30e-6 \text{ F}$ , and the load  $RL = 1 \Omega$ .



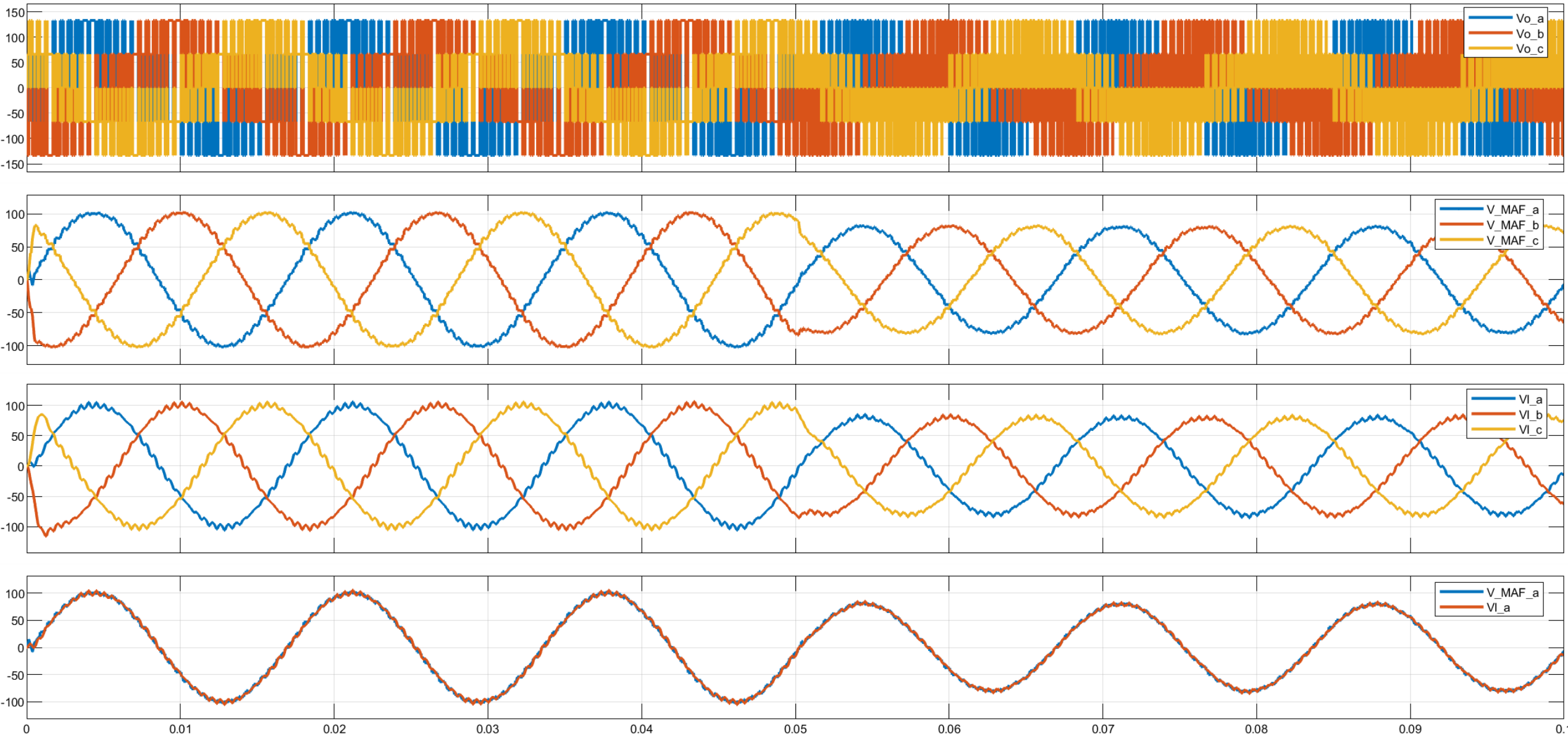


Figure 2.12: The converter voltage, the filtered converter voltage, and the PCC voltage.

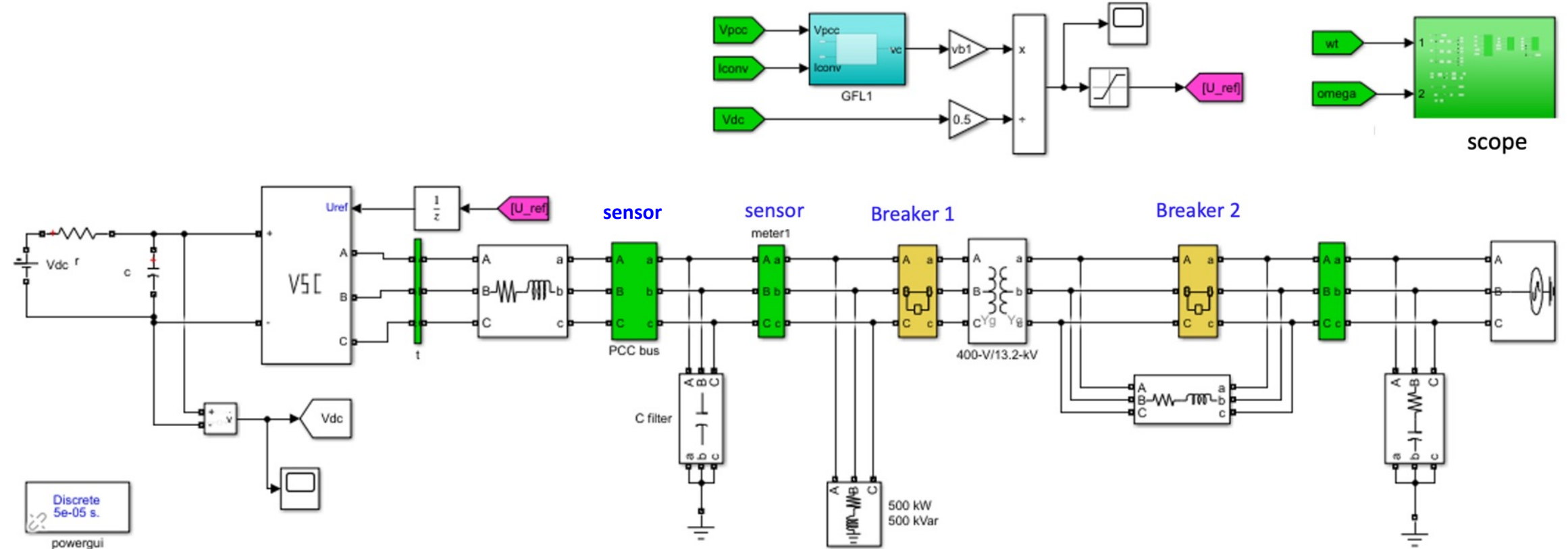


Figure 6.1 The EMT testbed implemented in MATLAB SPS

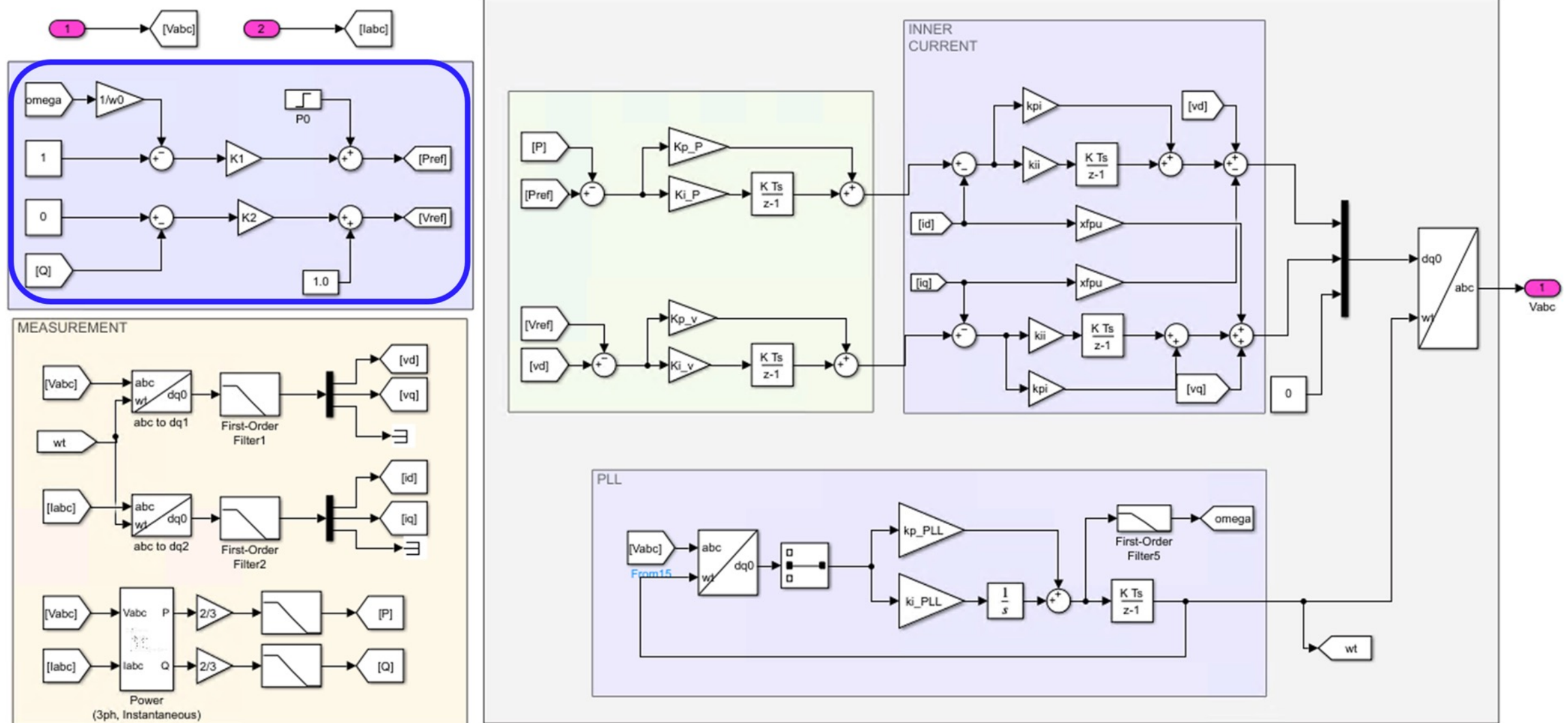


Figure 6.2: GFM1 implemented in MATLAB SPS. The highlighted part is the droop control.

Mode 1: **Before 1s**, the IBR is connected to a strong grid and sending out a low power.

Mode 2: **From 1s to 2s**, the IBR is connected to a strong grid and sending out full power.

Mode 3: **From 2s to 4s**, the IBR is connected to a weak grid and sending out full power.

Mode 4: **From 4s to 6s**, the IBR is working in the standalone mode to serve the load.

Mode 3: **From 6s to 8s**, the IBR is reconnected to the grid and working in Mode 3.

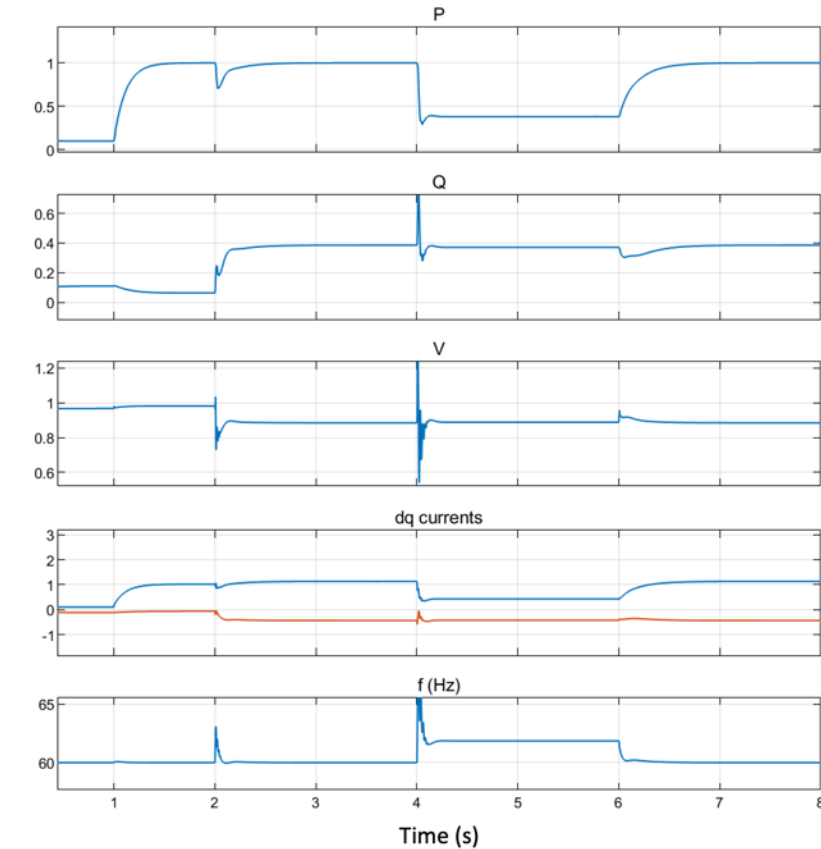


Figure 6.3: Simulation results of GFM1.

After  $t = 2$  s, line tripping,  $X_g = 0.8$  pu.

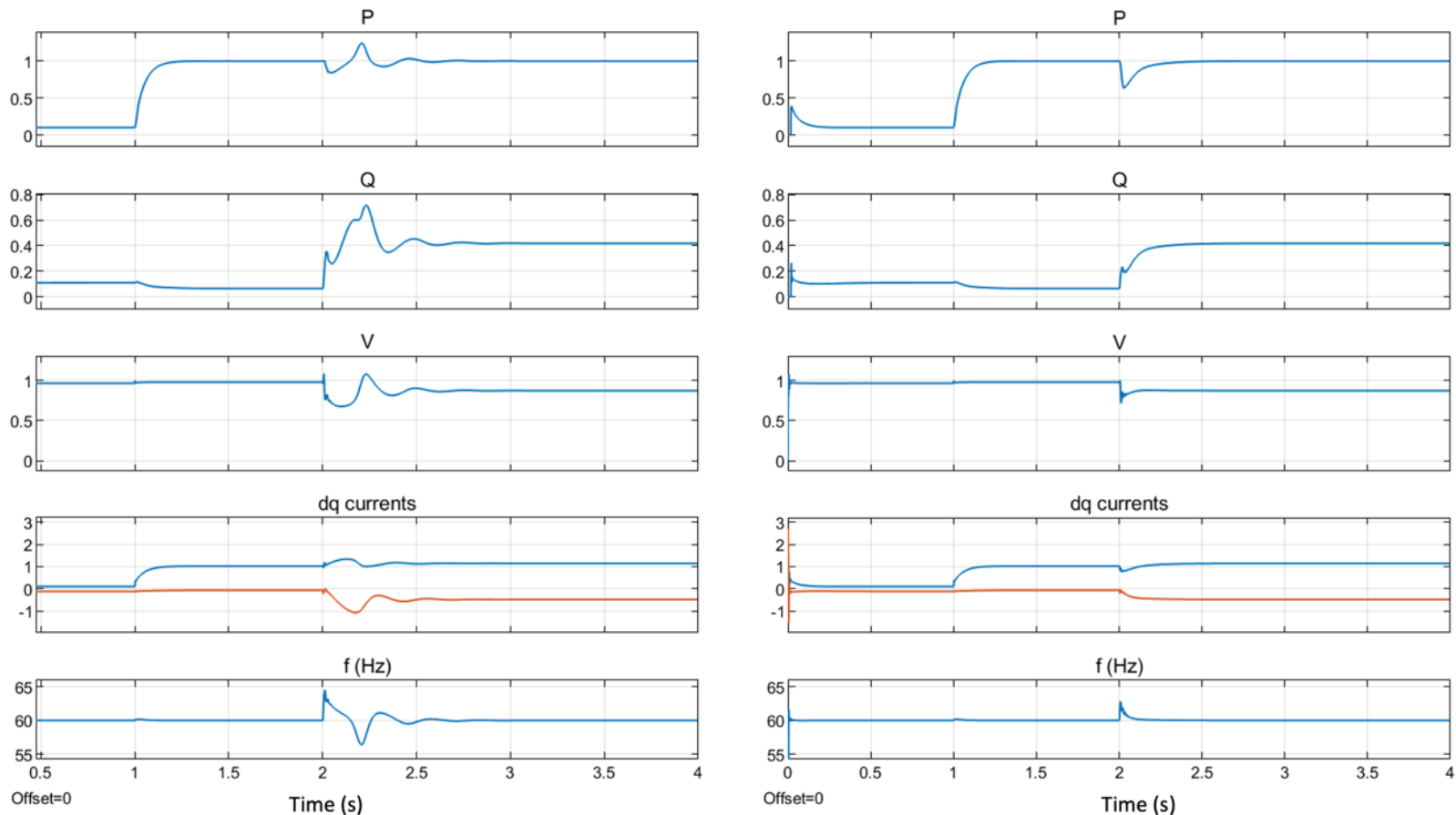


Figure 6.4: Simulation results of GFM1 **without and with the frequency droop control**. After  $t = 2$  s,  $X_g = 0.9$  pu. (a) marginally stable (b) stable

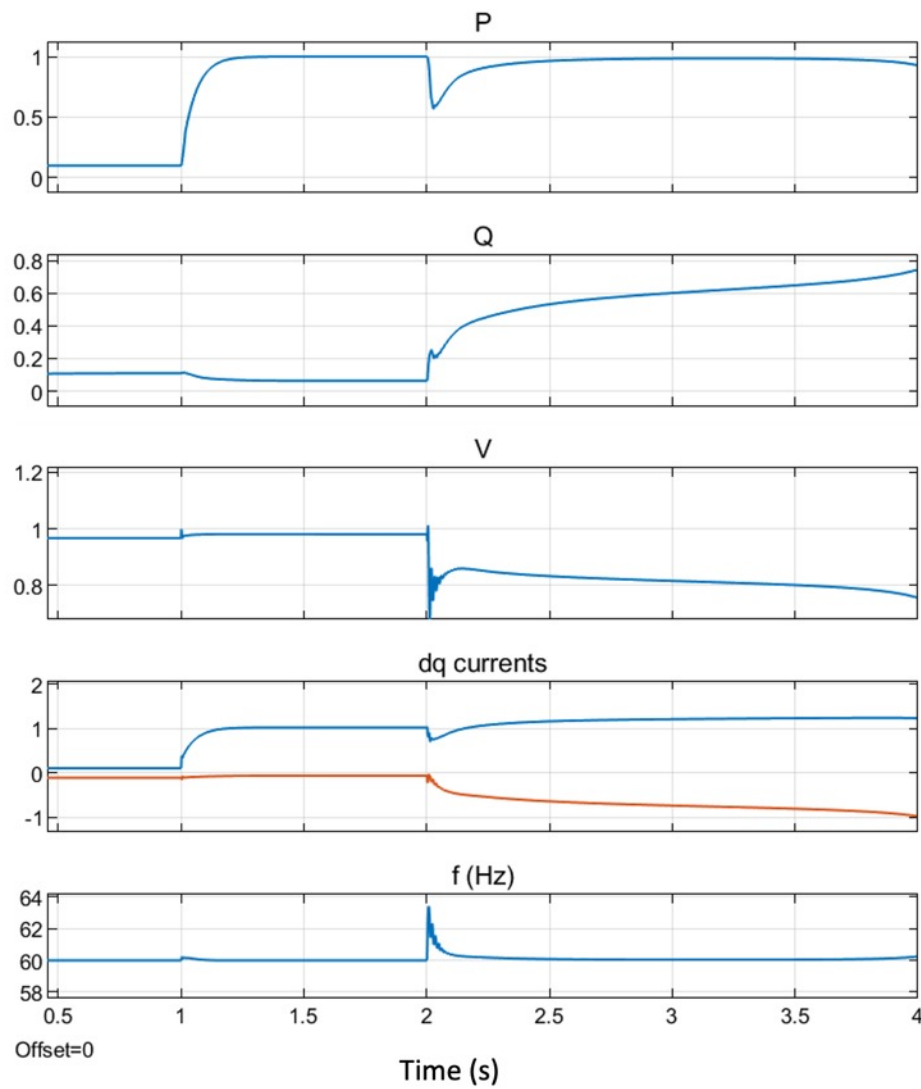
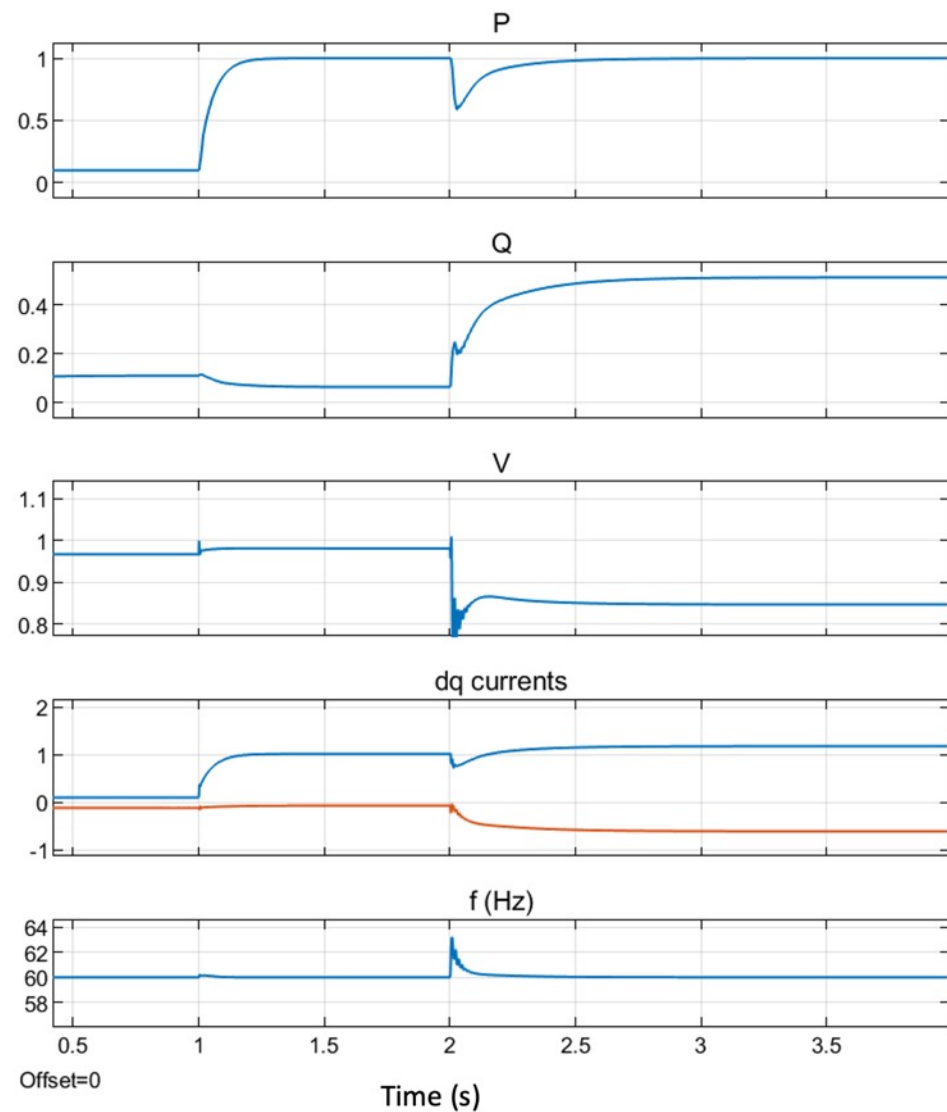


Figure 6.5: Simulation results of GFM1 with the frequency droop control when  $X_g = 1.1$  pu and  $X_g = 1.2$  pu after  $t = 2$  s, respectively.

Stability limit improves from  $X_g = 0.9$  to  $X_g = 1.2$  when the frequency droop control is added.

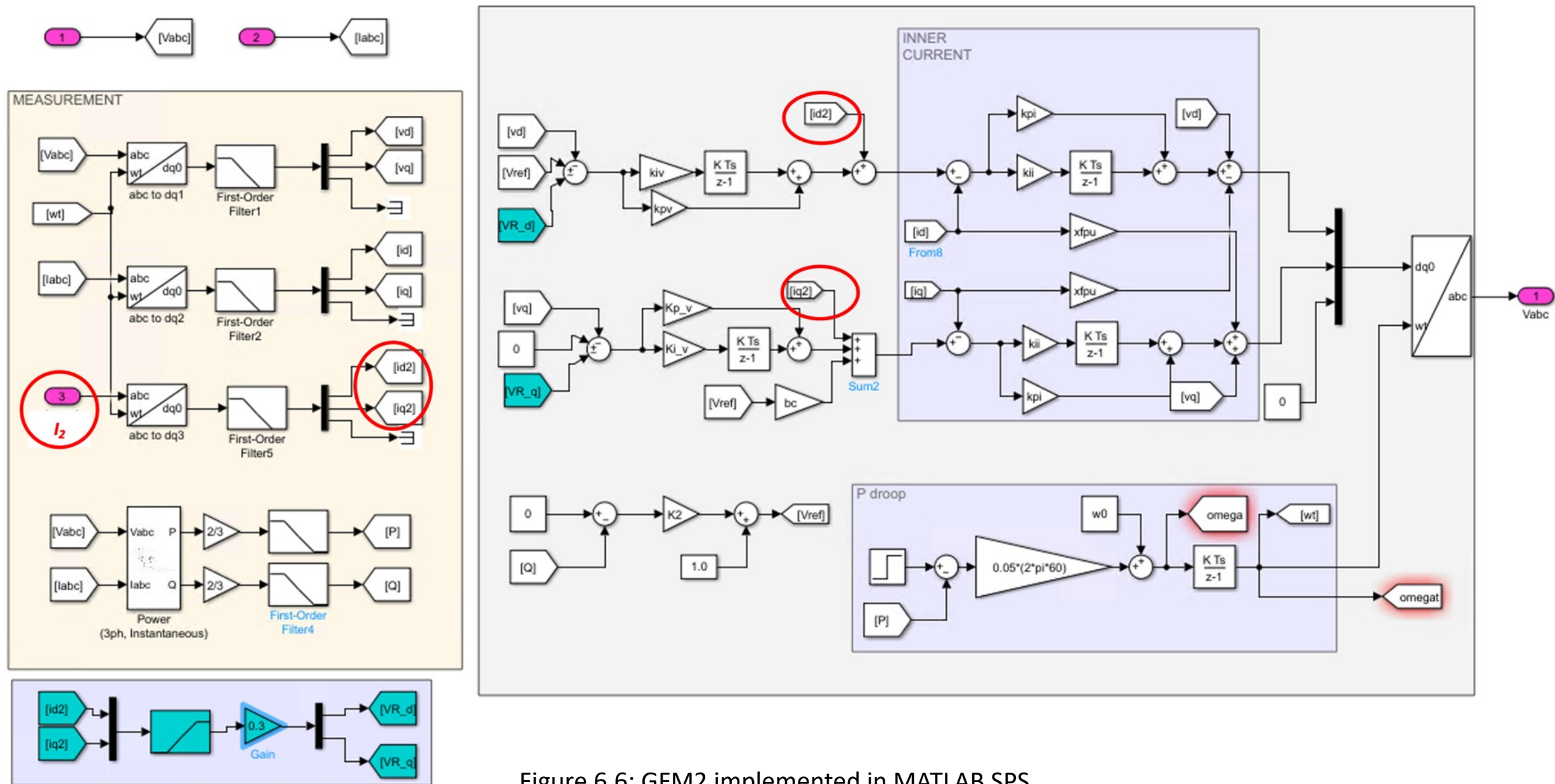


Figure 6.6: GFM2 implemented in MATLAB SPS.

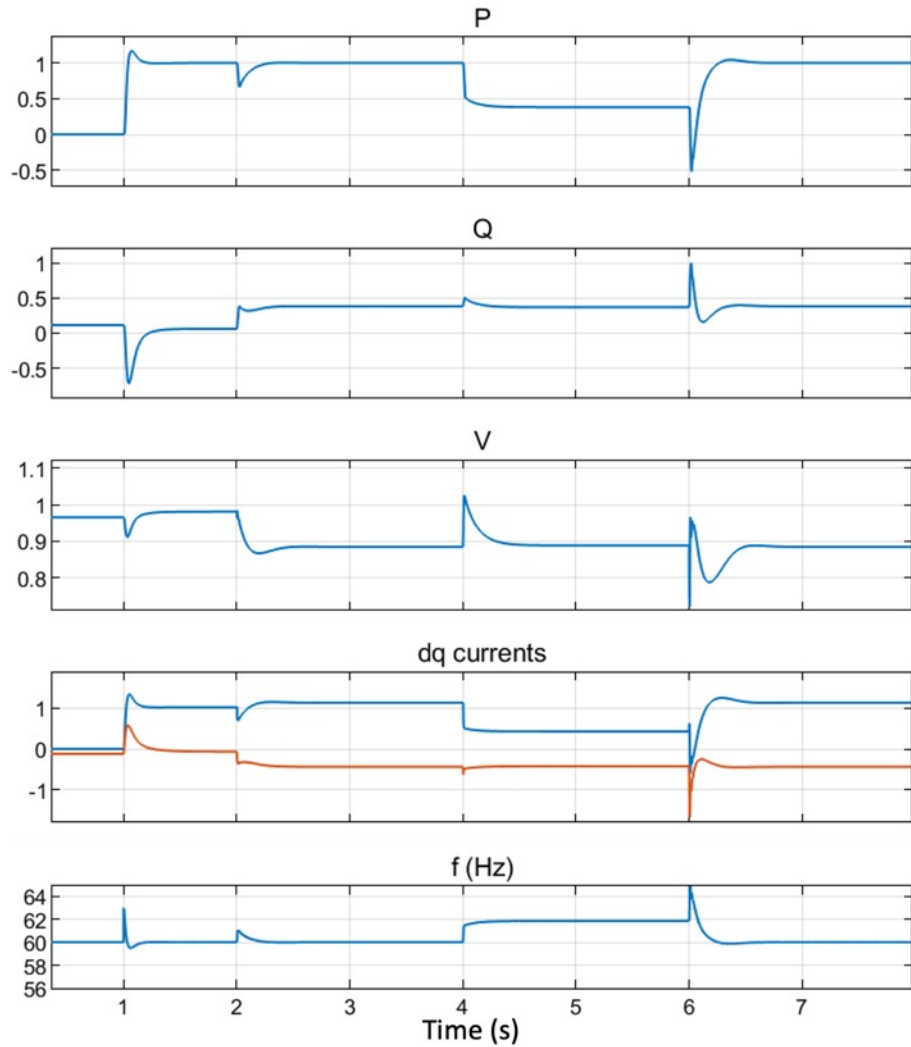


Figure 6.7: Simulation results of GFM2.

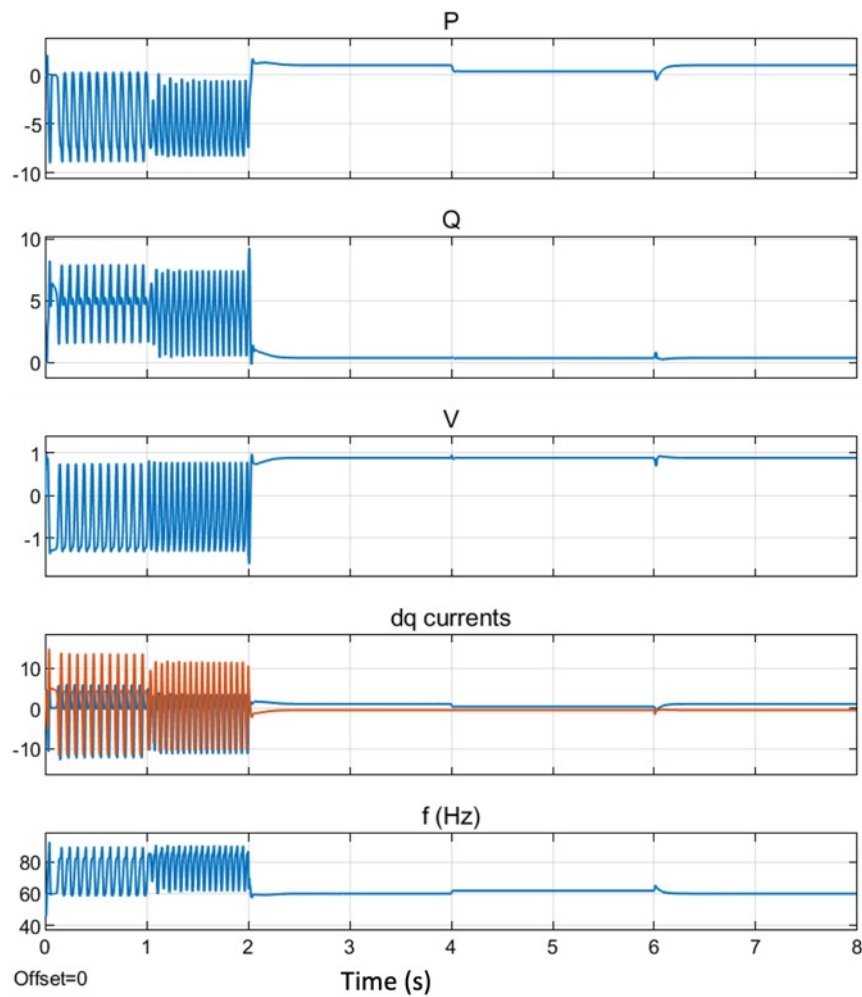


Figure 6.8: Simulation results of GFM2 if virtual resistor is not included.

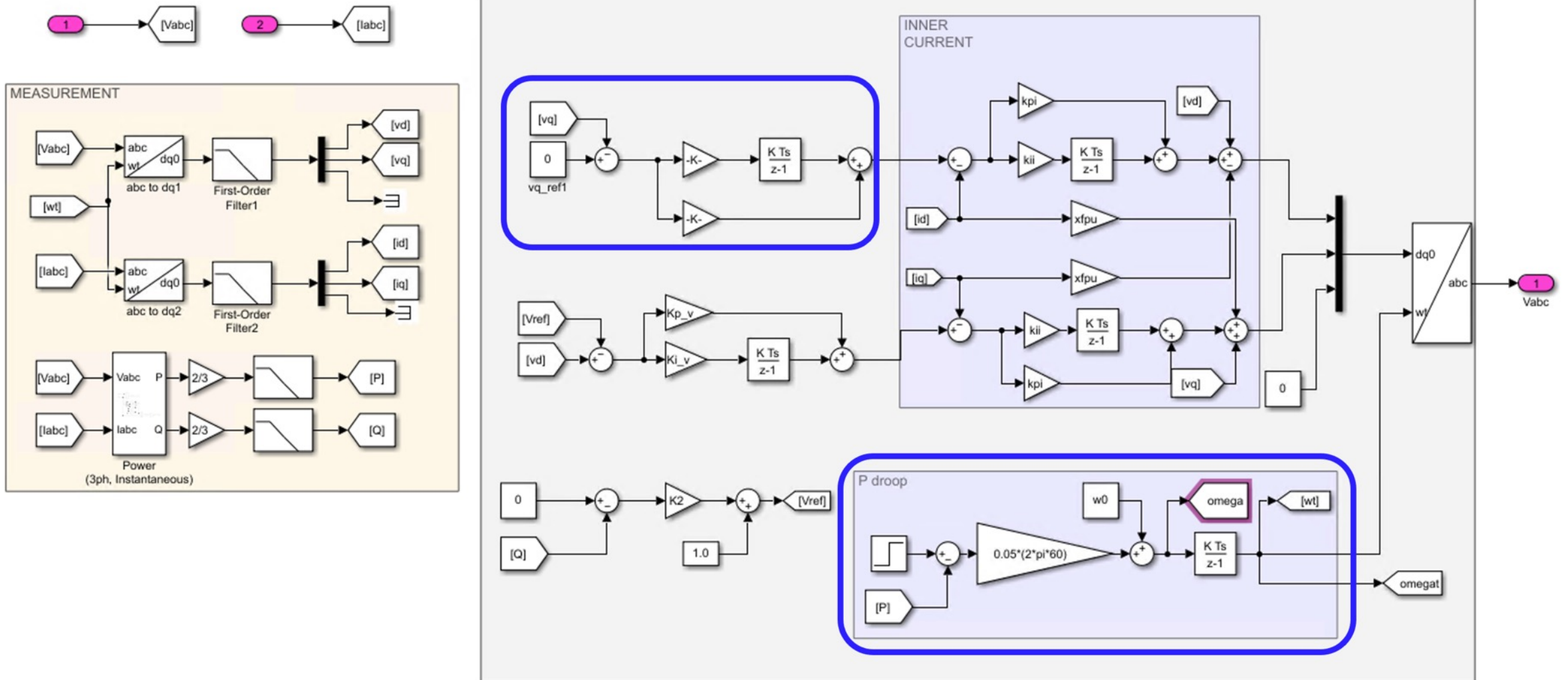


Figure 6.9: GFM3 (minimum edits) implemented in MATLAB SPS.

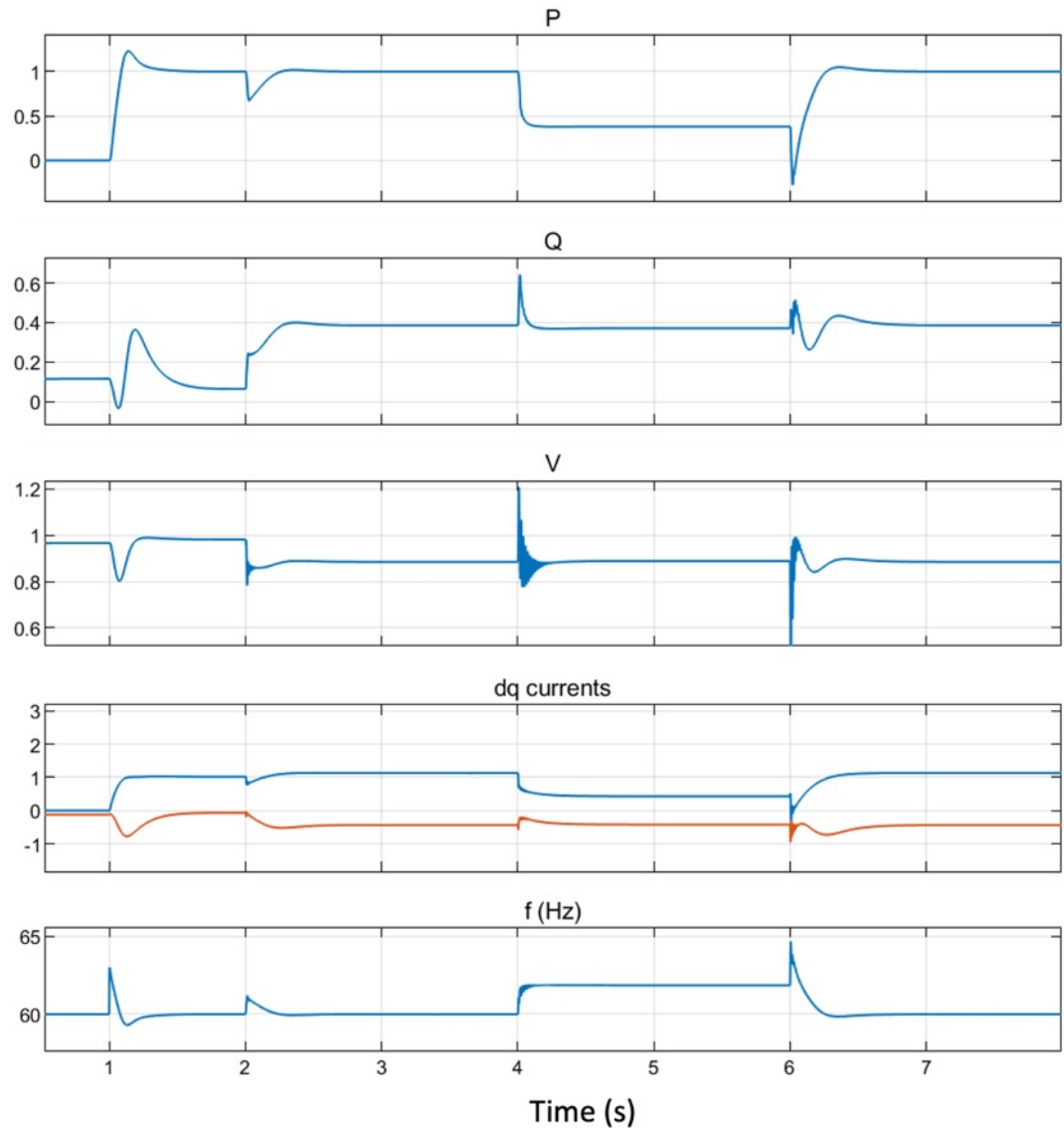


Figure 6.10: Simulation results of GFM3.

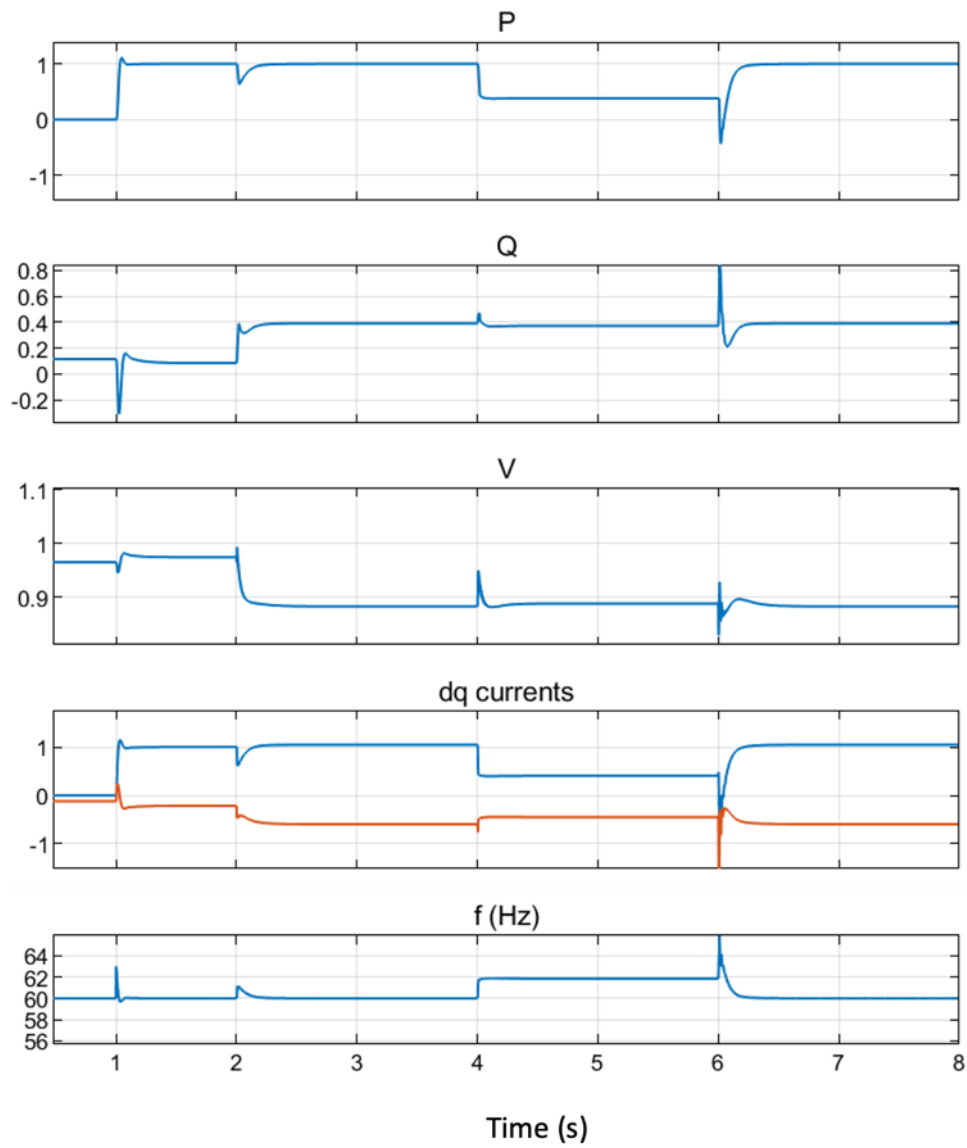


Figure 6.12: Simulation results of VSM.

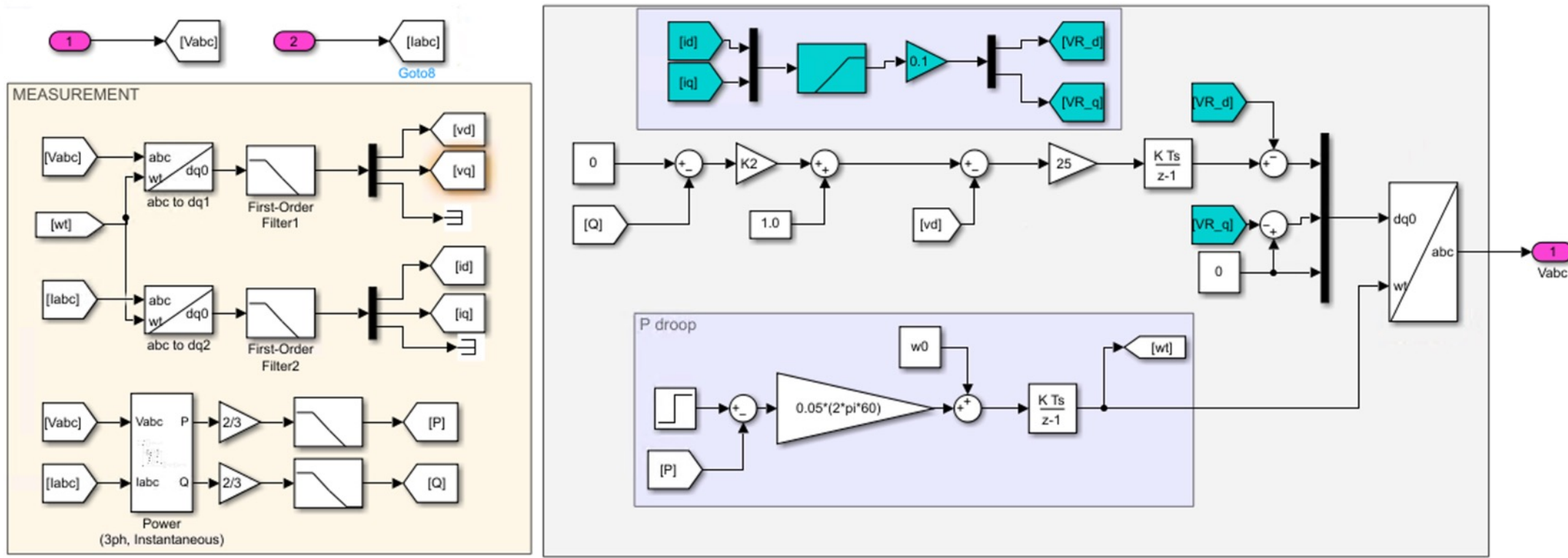


Figure 6.11: VSM (virtual synchronous machine) implemented in MATLAB SPS.

 **filseu** Update README.md03e93d4 · 4 months ago  History

Name	Last commit message	Last commit date
 ..		
 GFM_initial.m	Add files via upload	4 months ago
 README.md	Update README.md	4 months ago
 testbed_overall.slx	Add files via upload	4 months ago
<hr/>		
README.md		

## Chapter 6 Grid forming (GFM) control

6.1 Multi-loop GFM: from GFL to GFM

6.2 GFM1: advatanced GFL

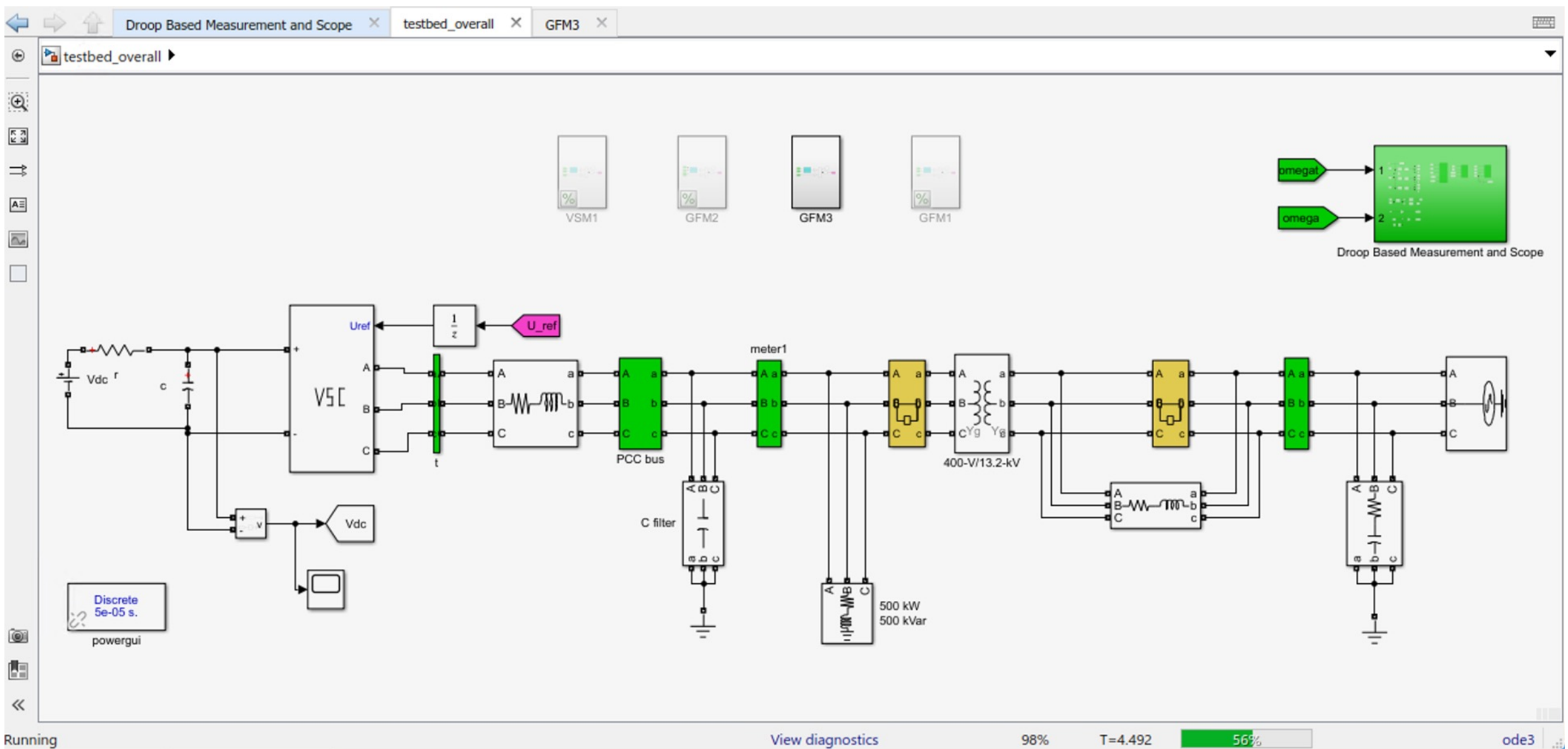
6.3 GFM2: the conventiaonl design (based on Yazdani's green book chapter 9)

6.4 GFM3: minimal edits - a new design

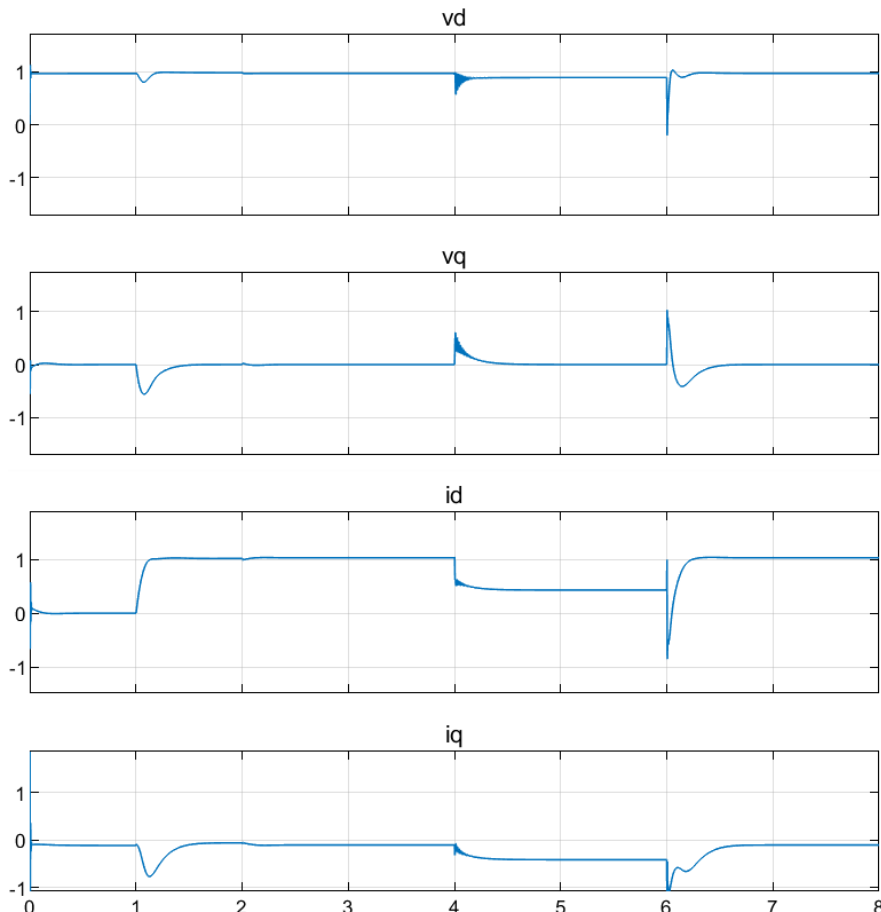
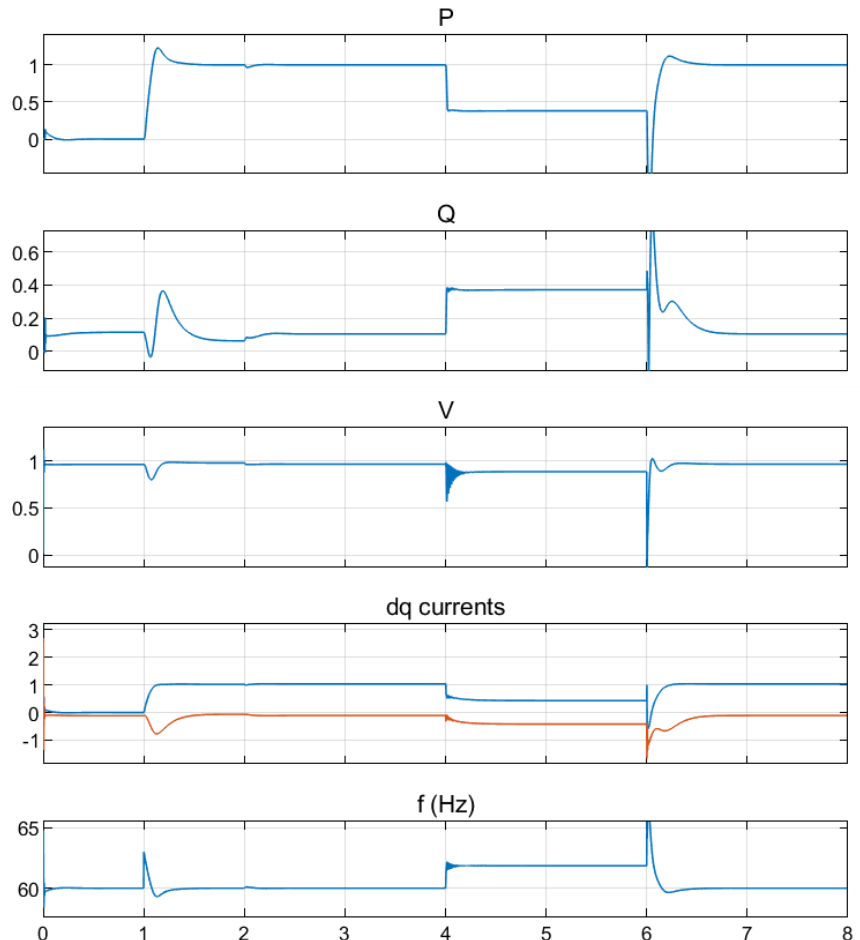
6.5 Virtual synchronous machines (VSM)

6.6 Summary

In this chapter, four testbeds (GFM1, GFM2, GM3, and VSM) are shown in Figs 6.2, 6.6, 6.9, 6.11. The foler contains one testbed that can be quickly turned into four differnt testbeds.



# EMT simulation results



Before 1 s, grid-connected operation.

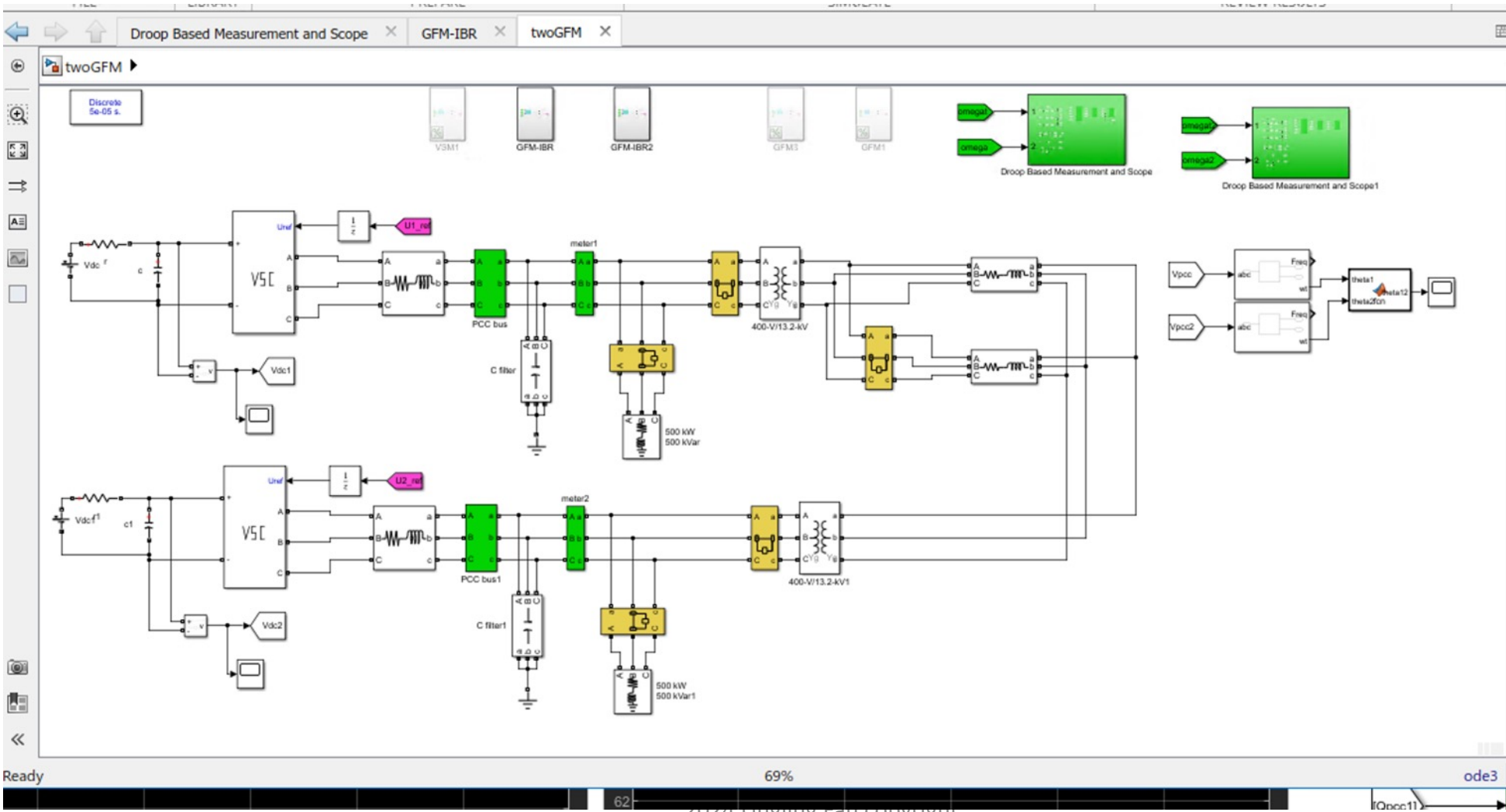
t = 1 s: P order ramp up to 1.

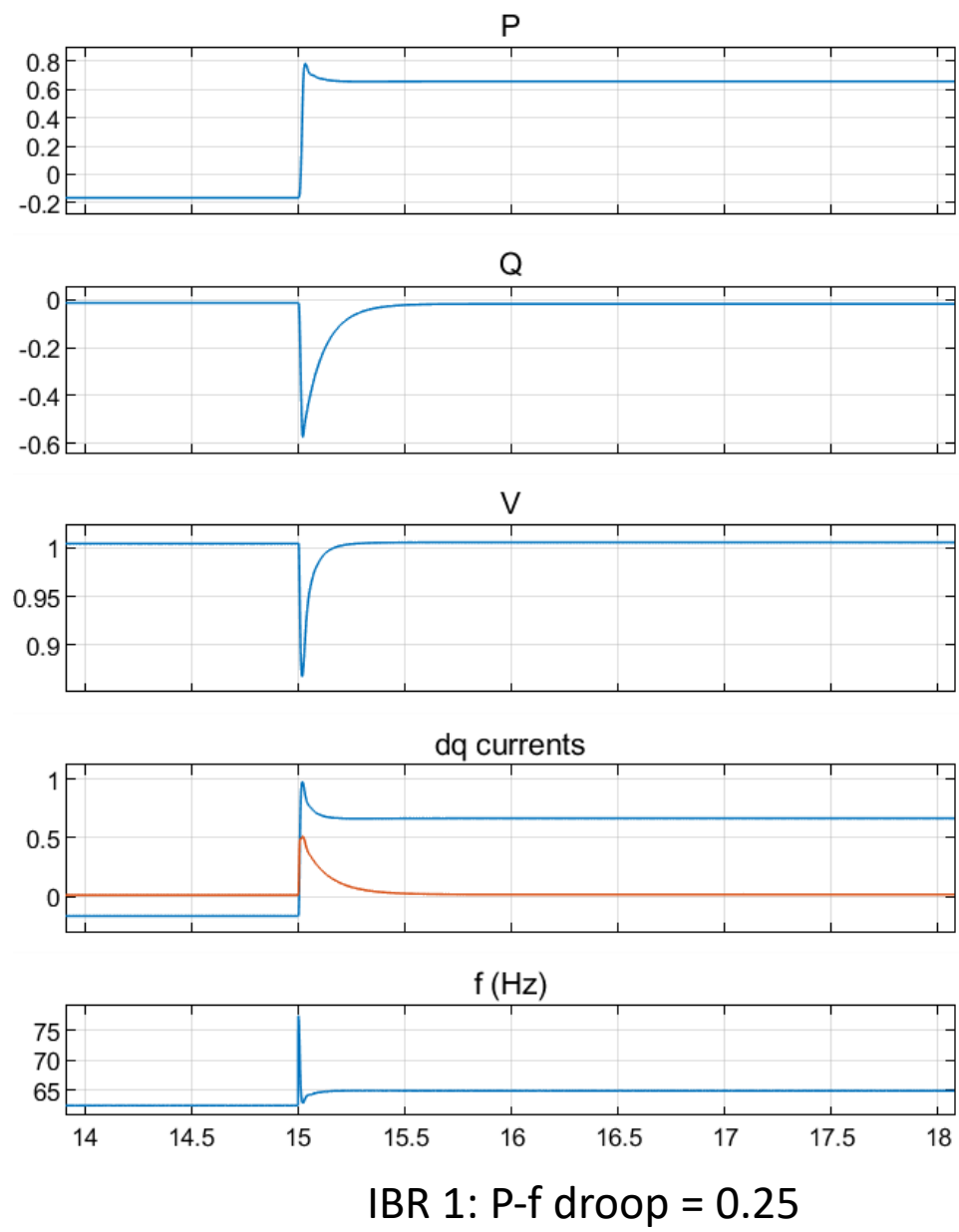
t = 4 s: Break off from the grid → standalone operation

t = 6 s: resynchronizing.

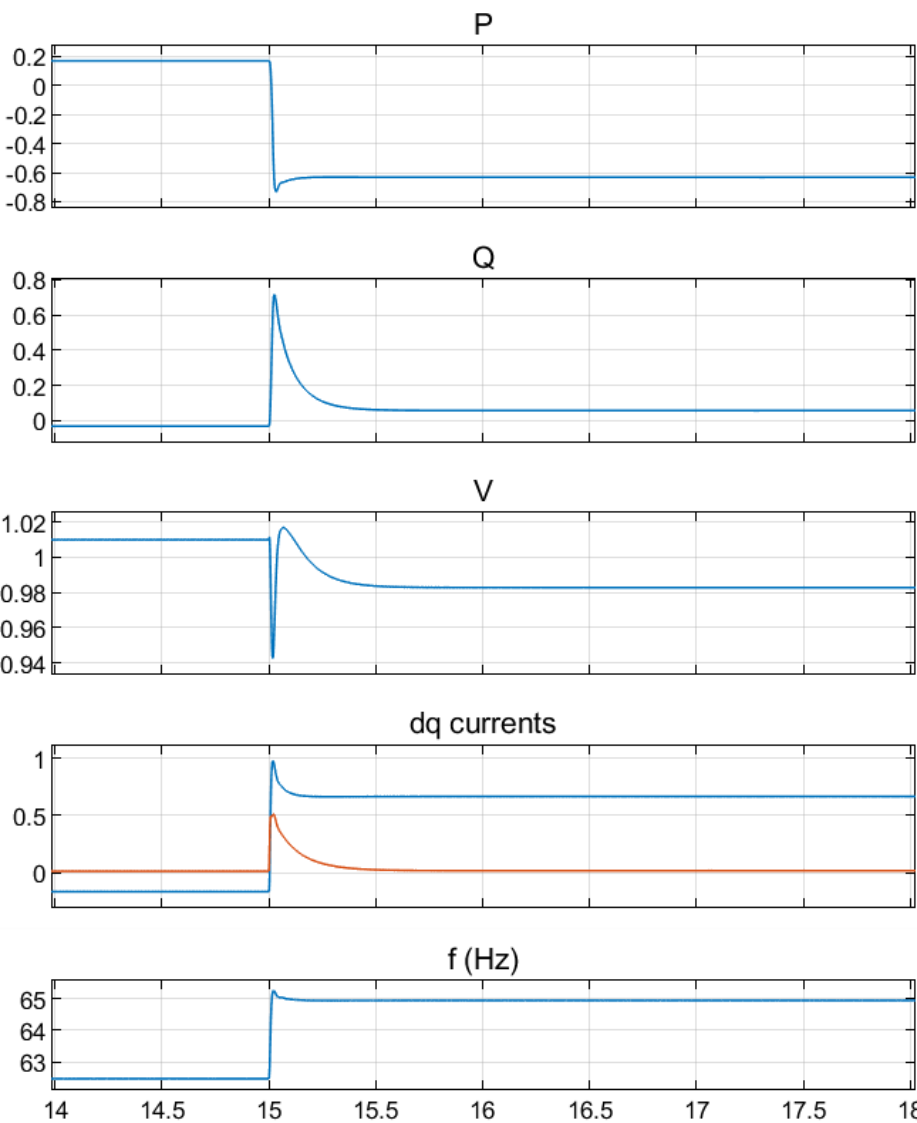
# Based on the single-IBR testbed in Github → Build multi-IBR testbeds

A Two-GFM testbed





$t = 15 \text{ s}$ , IBR1 power order from 0 to 1.  
 $\Delta f = (1-0.65)*0.25*60 \text{ Hz} = 5 \text{ Hz}$



IBR 2: P-f droop = 0.05  
 $\Delta f = (1+0.65)*0.05*60 \text{ Hz} = 5 \text{ Hz}$

$$= 5 \text{ H}$$

# Design & analysis: Feedback systems

1. voltage-var feedback system
2. GFM control design
3. GFM control loop tuning

# Chapter 5.2: analysis of real-world 0.1-Hz oscillation event

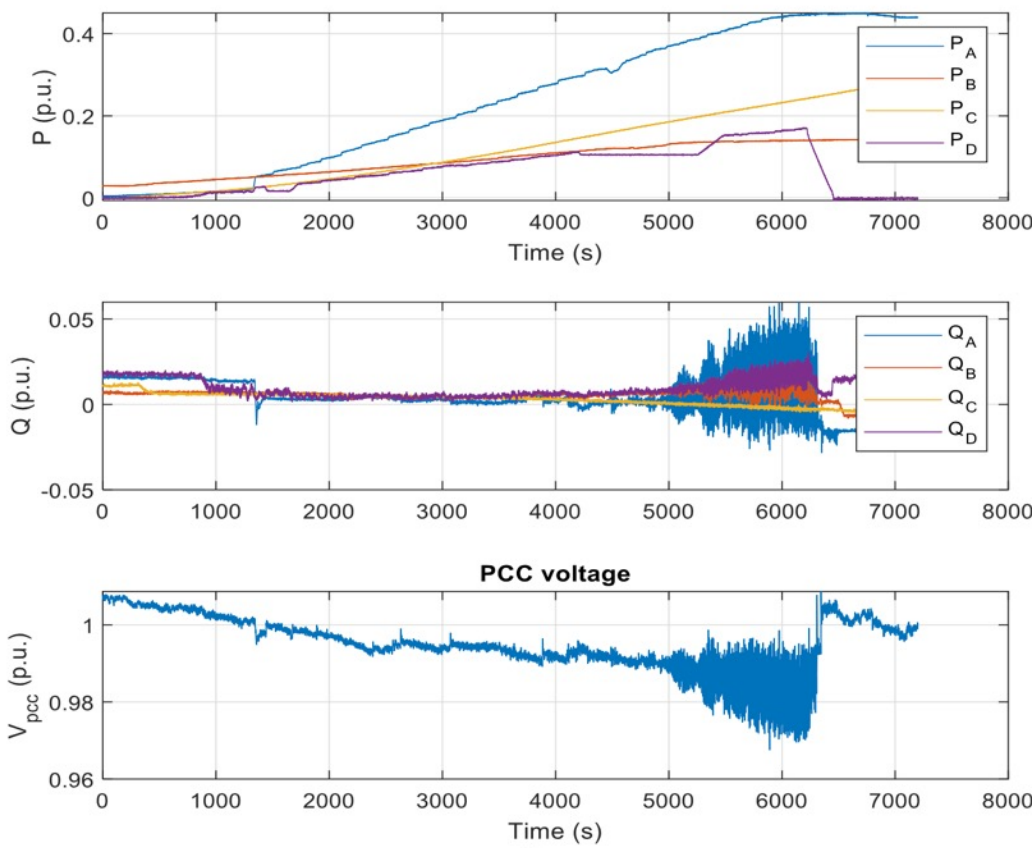


Figure 5.9 1-GW solar PV power plants 1-s interval SCADA measurements

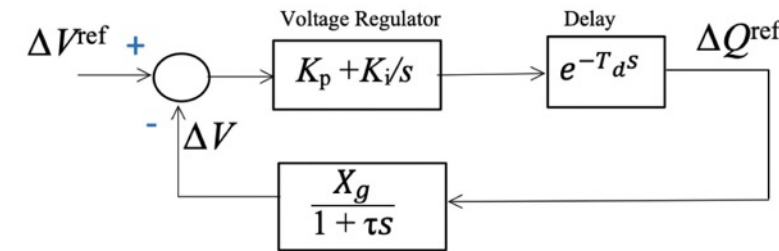


Figure 4.28 The voltage-var closed-loop system.

This feedback system cannot explain why real power ramping can cause 0.1-Hz oscillations.

Let's include the effect of power or active current:

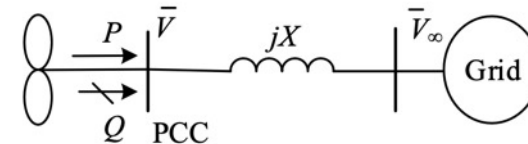


Figure 5.1: A single IBR infinite bus system.

$$\begin{aligned} v_d &= -Xi_q + V_\infty \cos \delta, \\ 0 &= v_q = +Xi_d - V_\infty \sin \delta. \end{aligned} \tag{5.2}$$

$$\Delta V = \Delta v_d = -X\Delta i_q - \underbrace{\frac{X}{\sqrt{\left(\frac{V_\infty}{Xi_d}\right)^2 - 1}}}_{c} \Delta i_d. \tag{5.5}$$

# Loop gain Bode diagram analysis

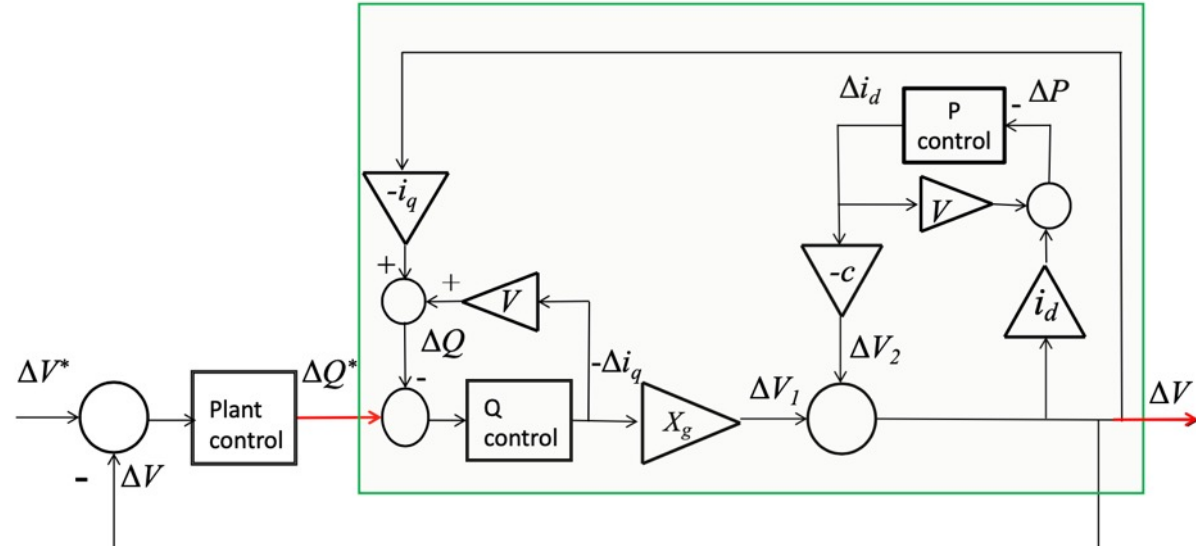


Figure 5.10 voltage-reactive power feedback system

An IBR power plant is assumed as a dq current source.

- When the delay is 4s, the system will see 0.1-Hz oscillations in voltage and reactive power.
- $V$  to  $P$  is a high-pass filter. Hence,  $P$  shows insignificant oscillations

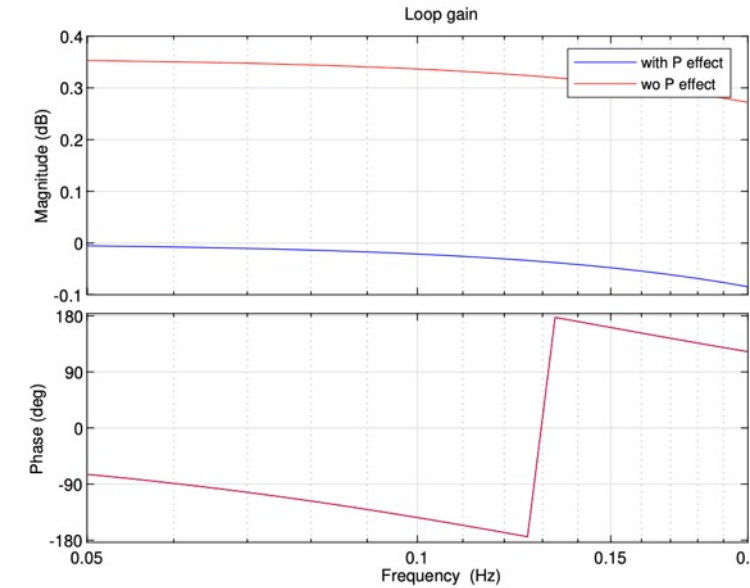


Figure 5.13: Bode diagrams of the loop gain with or without consideration of the effect of  $P$  and  $i_d$

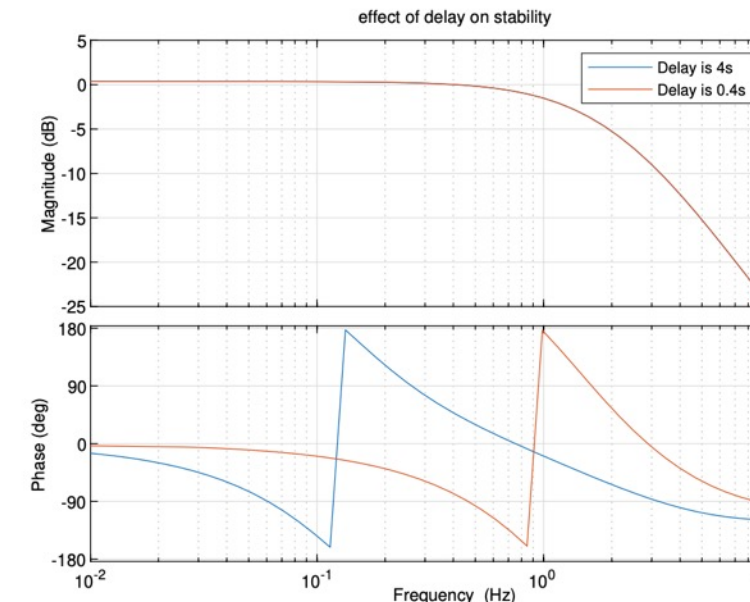


Figure 5.14: Effect of delay on the loop gain.

# GFM design (GFM3) : the minimal edits from GFL

1. PLL is replaced by a P-f droop control to generate the synchronizing angle.
2. P is now controlled by the P-f droop. The d-axis outer control needs to be updated.

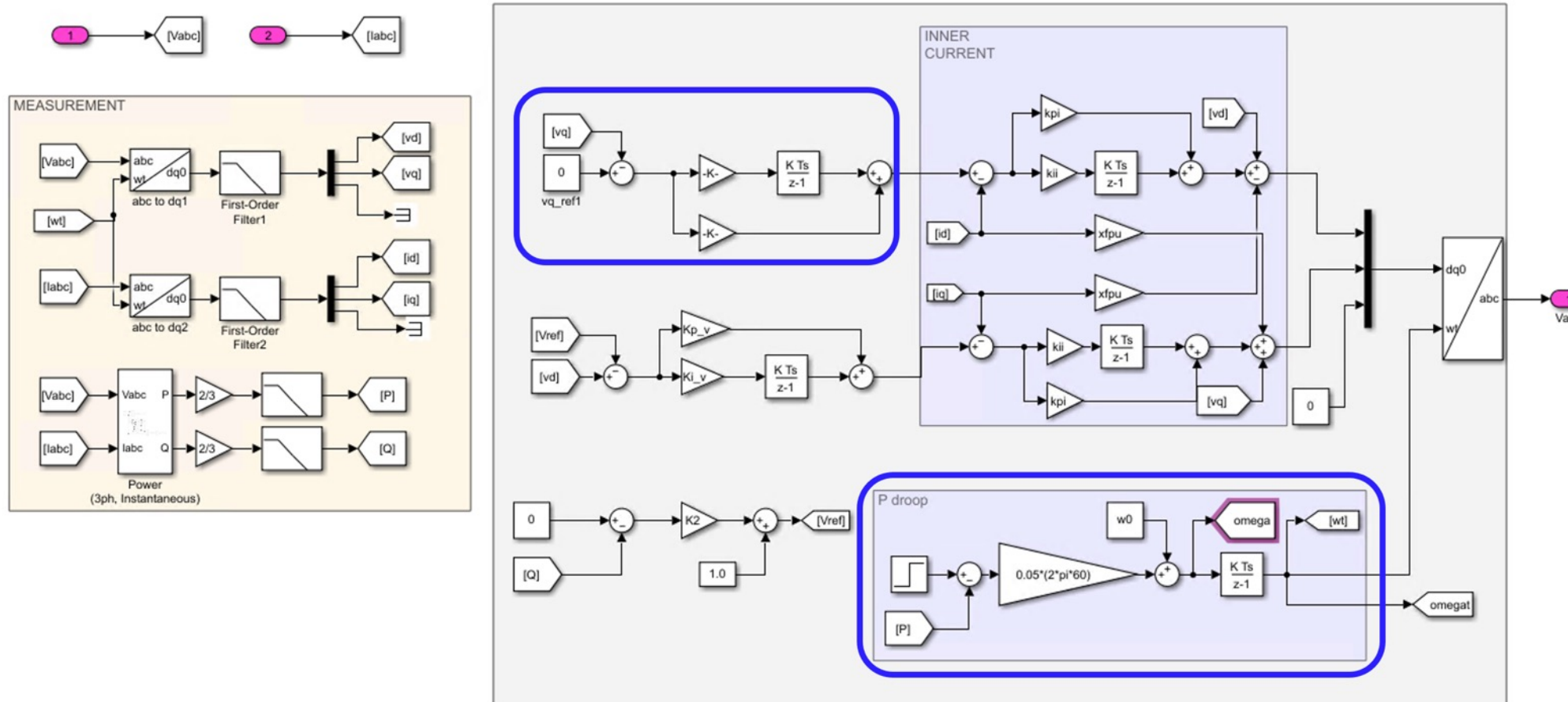


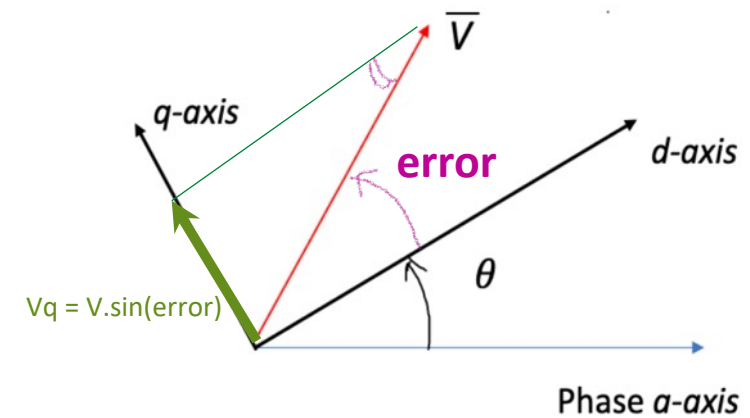
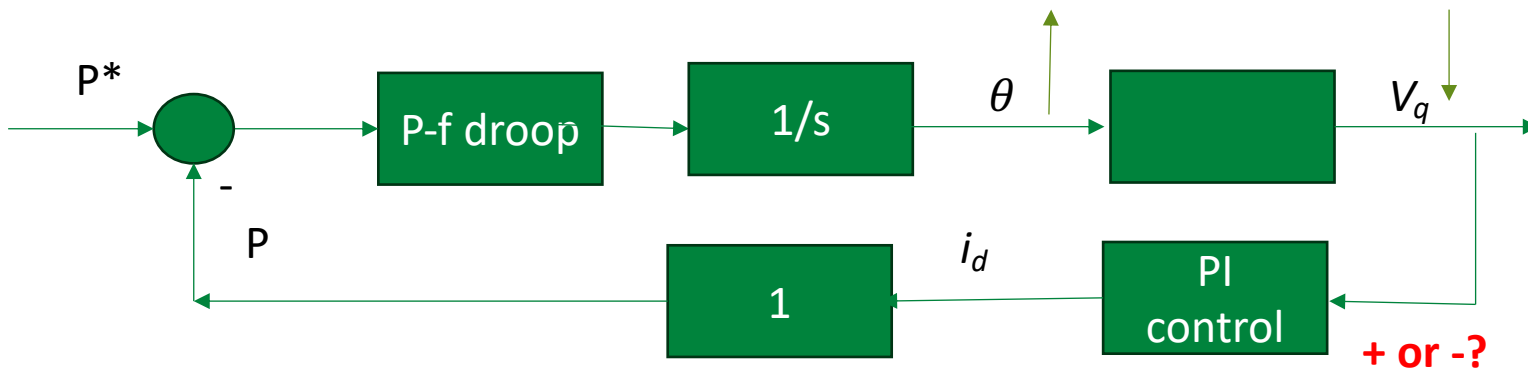
Figure 6.9: GFM3 (minimum edits) implemented in MATLAB SPS.

# How to design the d-axis control?

Need to enforce  $v_q = 0$  so that the synchronizing frame aligns with the PCC voltage space vector.

$Vq$ : angle between the PCC voltage space vector and the d-axis of the synchronizing frame.

$Vq$  control generates active current  $i_d^*$ , or influences real power



Based on this feedback system, if the  $P$  order increases, to make sure the  $P$  measurement can also increase, should  $Vq$  or  $-Vq$  be used as the input to generate  $i_d$ ?

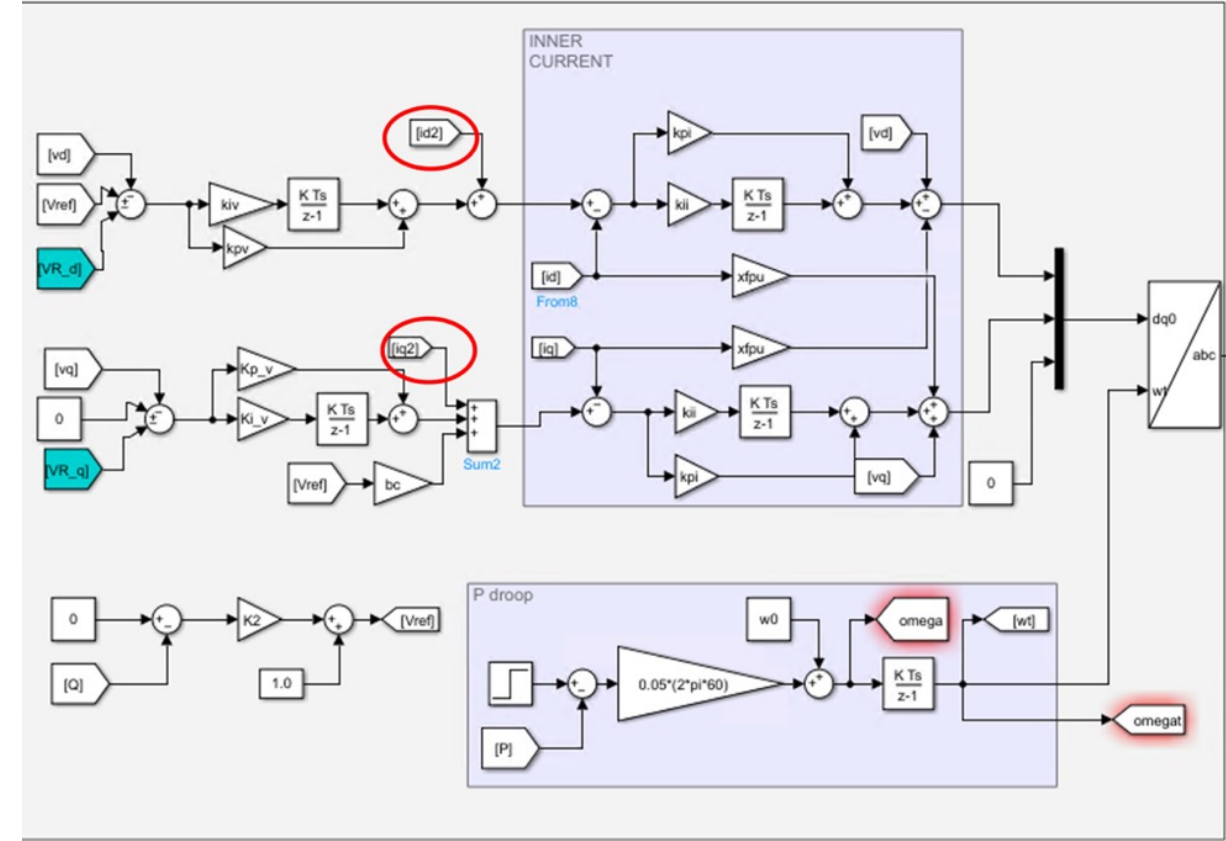
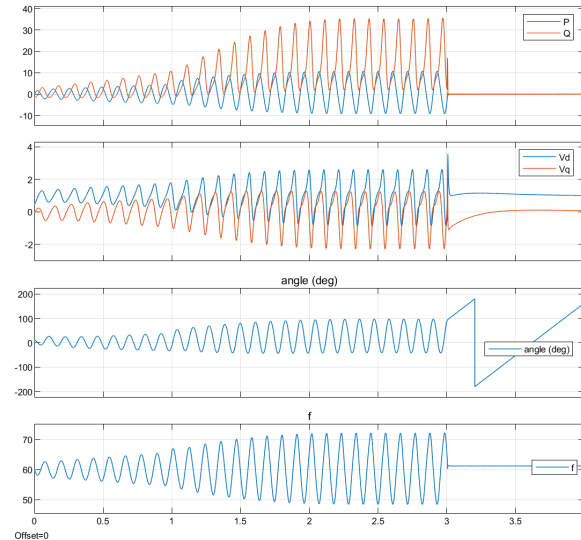
**- $Vq$  should be used as the input to the d-axis control.**

# System redesign for strong grids: GFM2 (conventional design)

Some common saying: GFM is good for weak grids but has issues with strong grids

One lesson learned: GFM needs careful parameter retune if its original design is for standalone operation instead of grid operation

- Based on a classic GFM design in Yazdani & Iravani's green book, power-frequency droop control is added to regulate frequency. Operating in the grid-connected conditions, the system is subject to oscillations when the grid is **strong**.
- The original design does not include the P-f control



EMT simulation results for  $X_g = 0.1$  pu and typical parameters designed based on the green book philosophy  
Outer PI control:  $0.1+0.1/s$

Outer control:  $0.4+40/s$

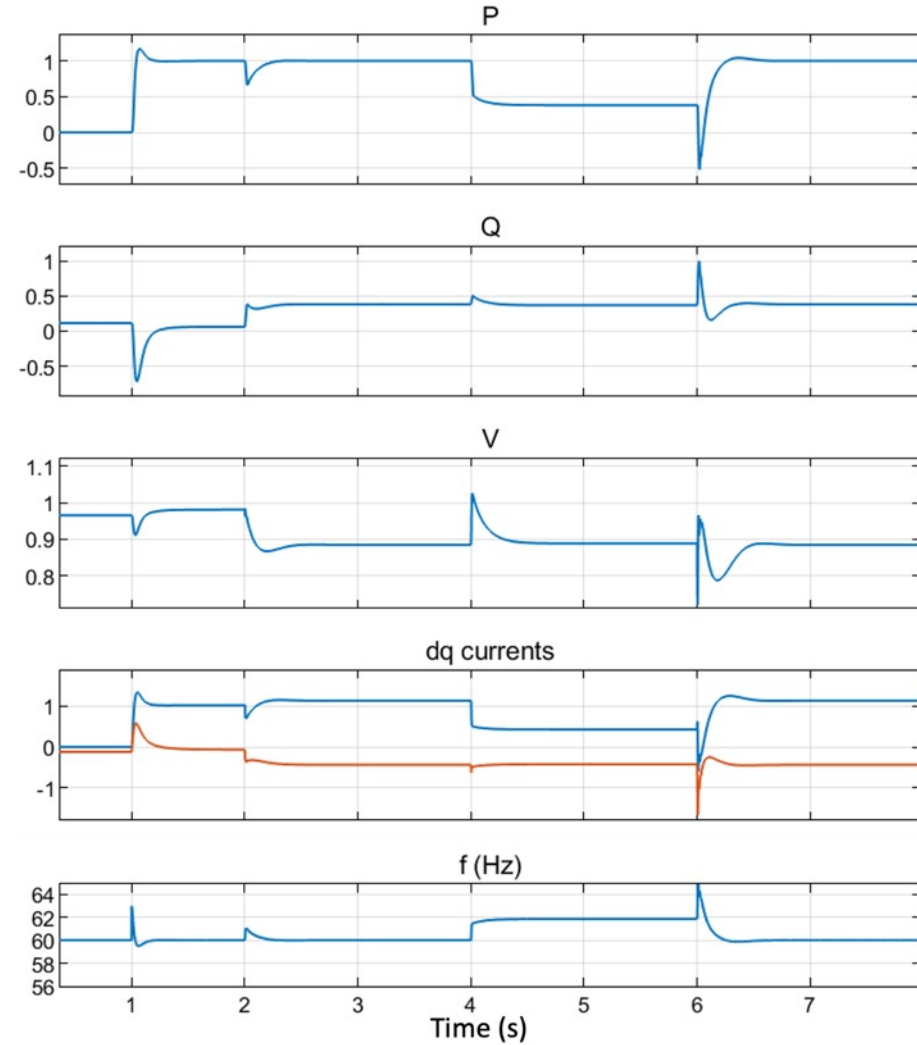


Figure 6.7: Simulation results of GFM2.

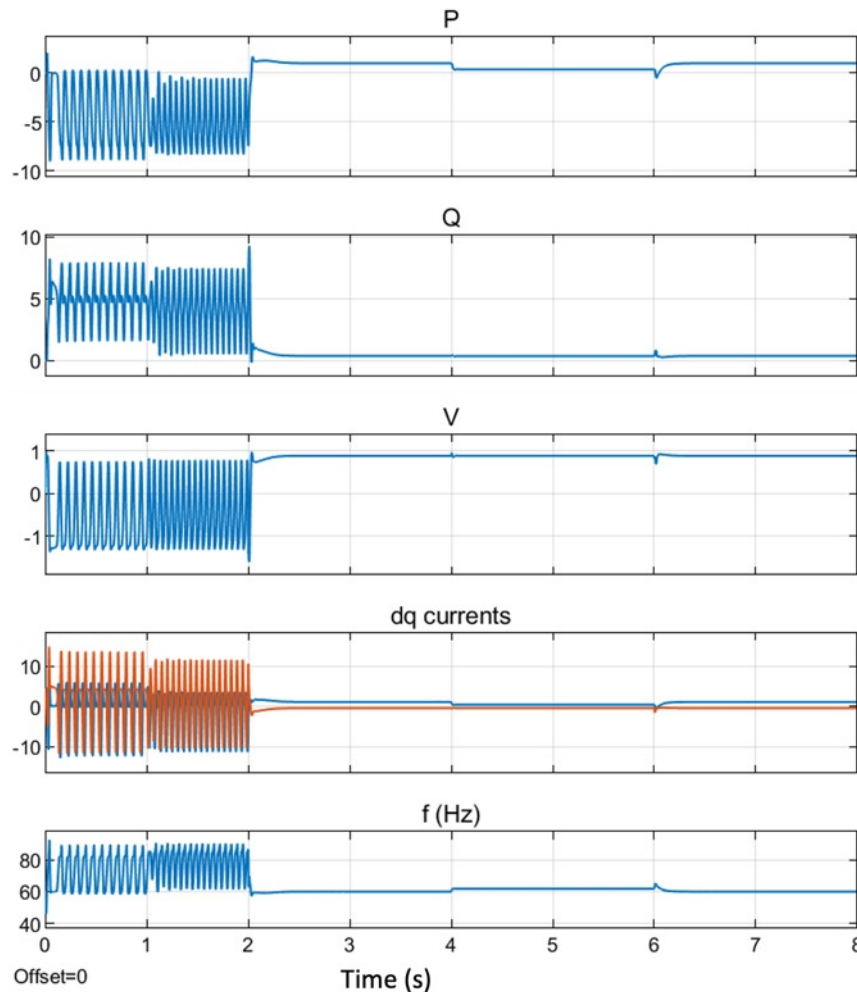
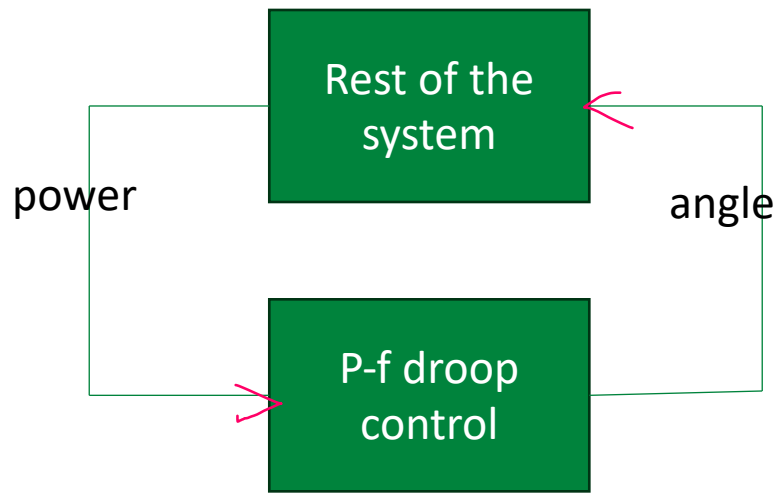


Figure 6.8: Simulation results of GFM2 if virtual resistor is not included.

# What is missing?

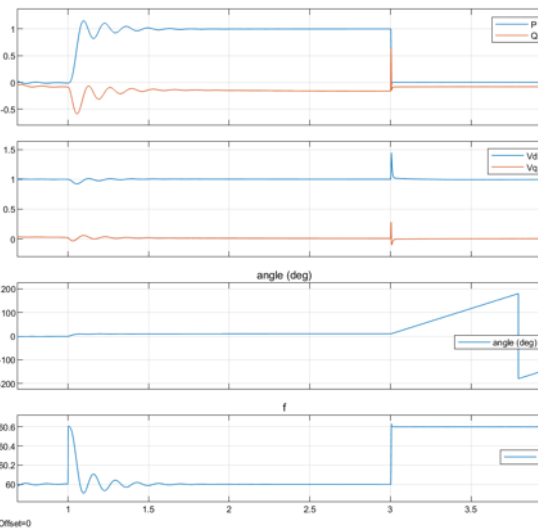
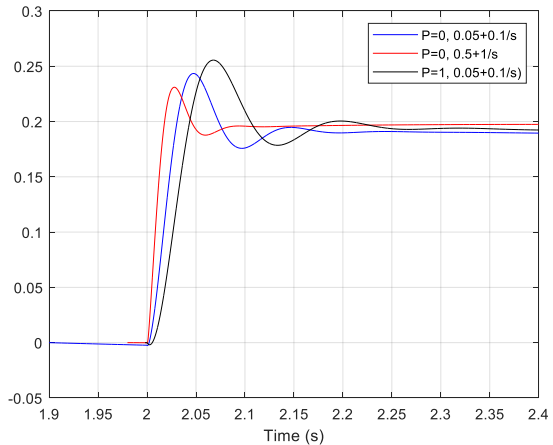


It is found that using the original parameters lead to slow power response upon a change in the synchronizing angle. Adding the effect of P-f droop control, oscillatory instability occurs.

**Mitigation:** Make power response to angle change faster; or make the PCC angle track the synchronizing angle faster. Identify the related control block & Increase the gain of that control. Issue solved!

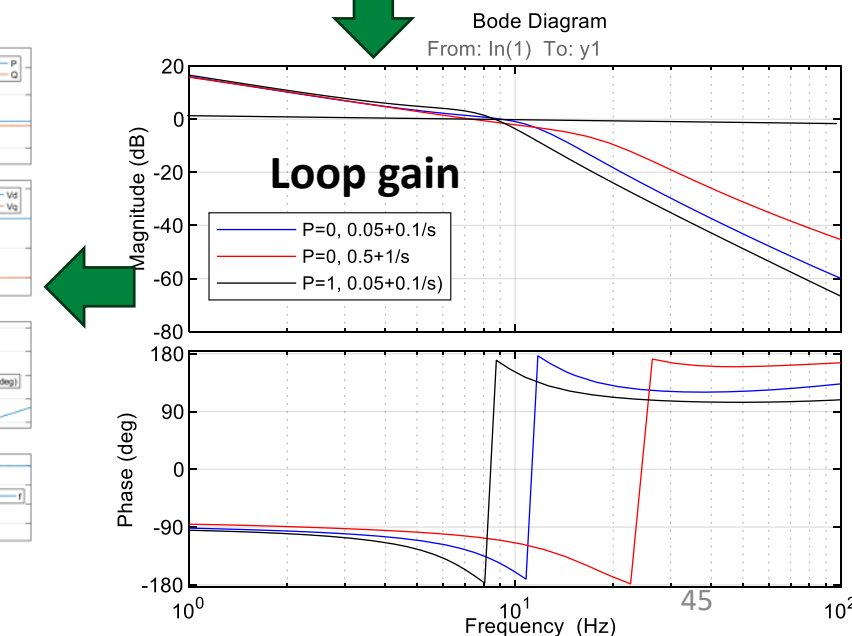
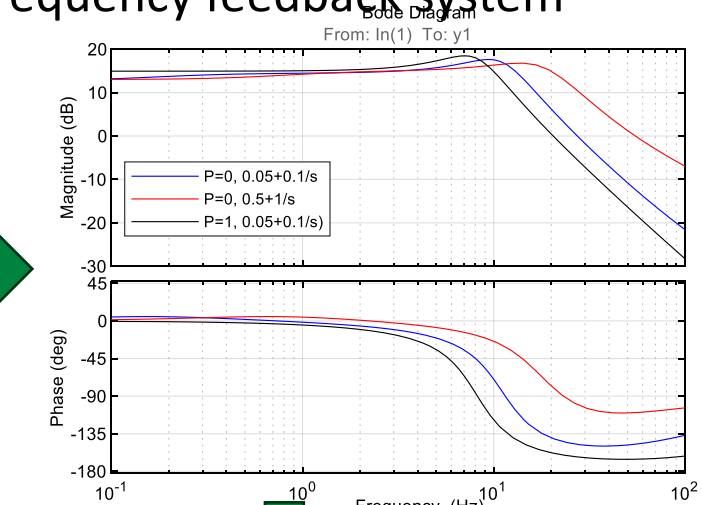
No need to virtual resistance.

## Check of power-frequency feedback system



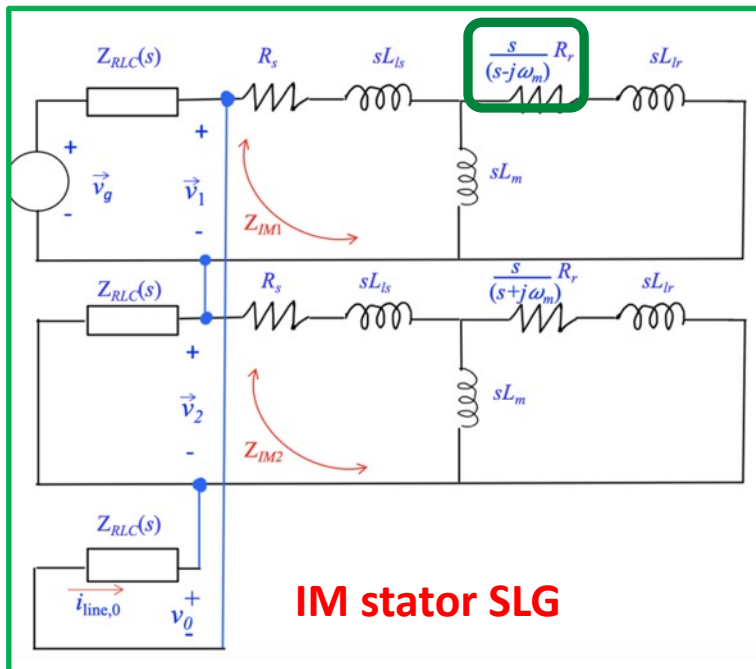
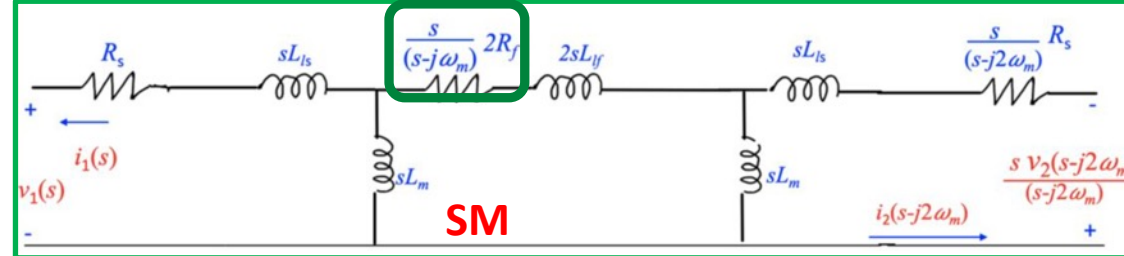
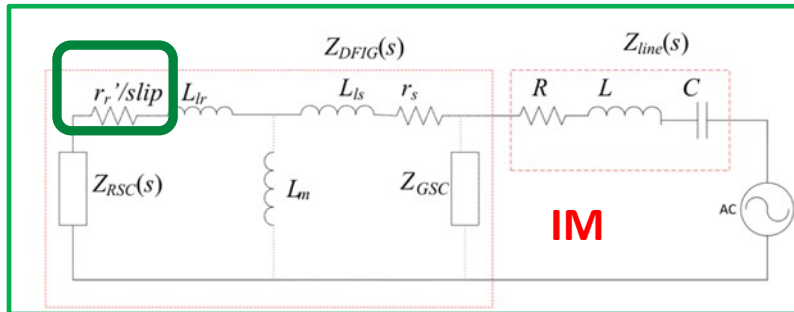
2024 Lingling Fan copyright

## Rest of the system



# S-domain circuits

# Chapter 9: Mechanism Analysis: constructing generalized dynamic circuits



➤ Z. Miao and L. Fan, "A Laplace-Domain Circuit Model for Fault and Stability Analysis Considering Unbalanced Topology," in IEEE Transactions on Power Systems, doi: 10.1109/TPWRS.2022.3230564.

- ✓ An induction (or synchronous) machine has **negative resistance** at subsynchronous frequency region.
- ✓ Unbalanced grid condition mitigates the negative resistance, thus improving stability

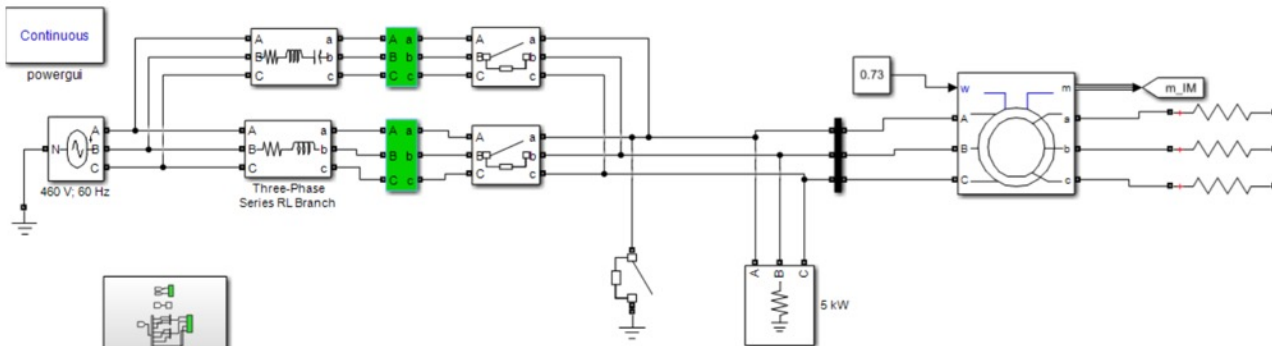
## Modeling & Mechanism Analysis:

- L. Fan and Z. Miao, "Nyquist-stability-criterion-based SSR explanation for type-3 wind generators," IEEE trans. Energy Conversion, vol. 27, no. 3, pp. 807–809, 2012.
- Miao Z. Impedance-model-based SSR analysis for type 3 wind generator and series-compensated network. IEEE Transactions on Energy Conversion. 2012 Aug 23;27(4):984-91.
- L. Fan, Z. Miao, "Analytical model building for Type-3 wind farm subsynchronous oscillation analysis". Electric Power Systems Research, 2021, p.107566.

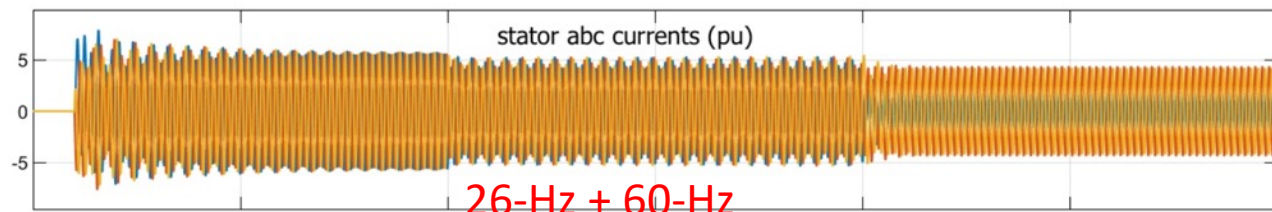
## Control solutions:

- L. Fan, Z. Miao. "Mitigating SSR using DFIG-based wind generation." IEEE TSTE 2012
- Y. Li, L. Fan, Z. Miao. "Replicating real-world wind farm SSR events." IEEE TPWRD 2018

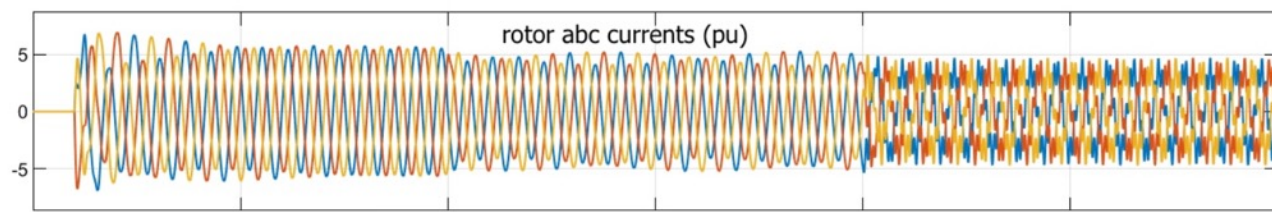
# SLG fault mitigates SSR



(a)



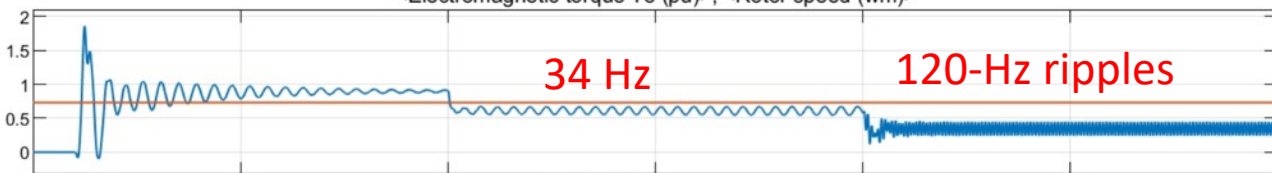
26-Hz + 60-Hz



<Electromagnetic torque Te (pu), <Rotor speed (wm)>

34 Hz

120-Hz ripples



(b)

Figure 9.10:

- (a) An induction motor connected to a series compensated network is subject to unbalanced fault.
- (b) Simulation results. Before  $t = 1$  s, the motor is connected to both the RL and the RLC circuits. At  $t = 1$  s, the parallel RL circuit is tripped leaving the motor radially connected to the RLC circuit. At  $t = 2$ , phase  $a$  is connected to the ground.

## Dynamic circuits for unbalanced topologies

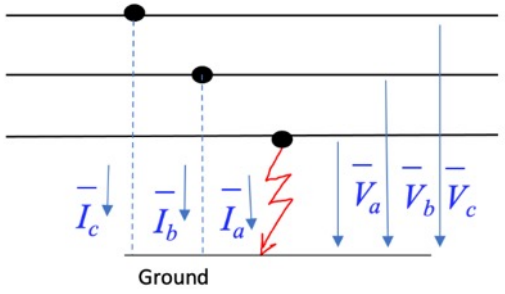
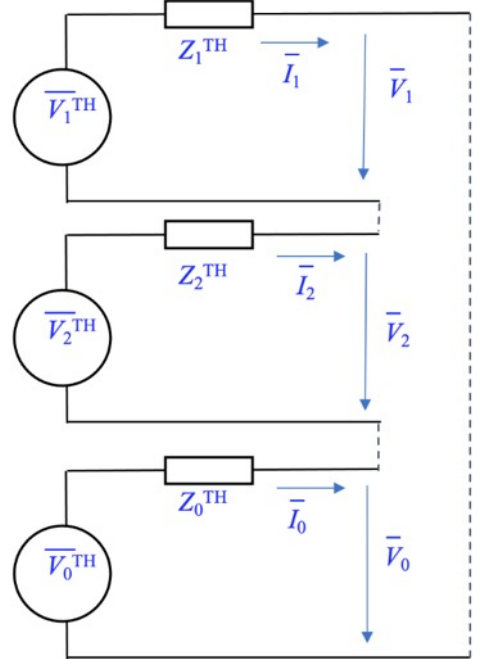


Figure 9.9: Sequence networks interconnected in series for an SLG fault.



$$\frac{\vec{v}}{2} = \frac{1}{3} \left( v_a + e^{j\frac{2\pi}{3}} v_b + e^{-j\frac{2\pi}{3}} v_c \right), \quad (9.33)$$

$$\frac{(\vec{v})^*}{2} = \frac{1}{3} \left( v_a + e^{-j\frac{2\pi}{3}} v_b + e^{j\frac{2\pi}{3}} v_c \right), \quad (9.34)$$

$$v^0 = \frac{1}{3} (v_a + v_b + v_c). \quad (9.35)$$

$$\begin{aligned} v_a &= v^0 + \frac{\vec{v}}{2} + \frac{(\vec{v})^*}{2}, \\ v_b &= v^0 + e^{-j\frac{2\pi}{3}} \frac{\vec{v}}{2} + e^{j\frac{2\pi}{3}} \frac{(\vec{v})^*}{2}, \\ v_c &= v^0 + e^{j\frac{2\pi}{3}} \frac{\vec{v}}{2} + e^{-j\frac{2\pi}{3}} \frac{(\vec{v})^*}{2}. \end{aligned}$$

$$v_a = 0, \implies \frac{\vec{v}}{2} + \frac{(\vec{v})^*}{2} + v^0 = 0,$$

$$i_b = i_c = 0, \implies \frac{\vec{i}}{2} = \frac{(\vec{i})^*}{2} = i^0 = \frac{1}{3} i_a.$$

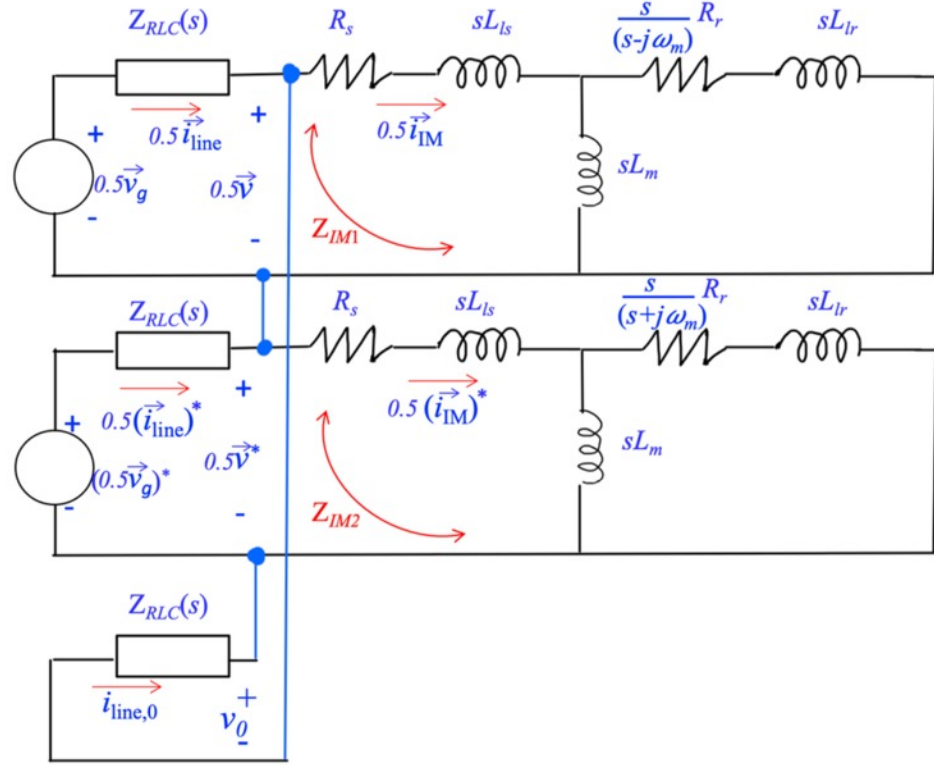


Figure 9.11: Circuit 1: the example system subject to an SLG fault.

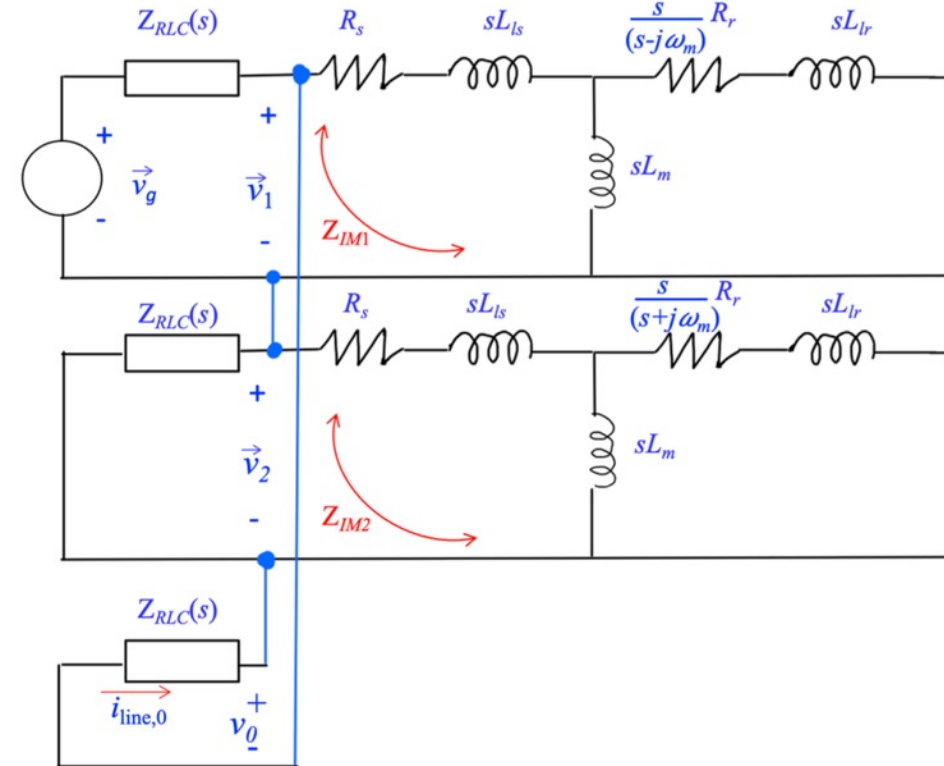


Figure 9.12: Circuit 2: the example system subject to an SLG fault.

SLG topology makes complex conjugate  $Z_{IM1}$  and  $Z_{IM2}$  parallel. **No more negative resistance.**

# QUESTIONS?

# References

- Fan, L., & Miao, Z. (2023). Modeling and Stability Analysis of Inverter-Based Resources (1st ed.). CRC Press. <https://doi.org/10.1201/9781003323655>
- Taylor & Francis:  
<https://www.taylorfrancis.com/books/mono/10.1201/9781003323655/modeling-stability-analysis-inverter-based-resources-lingling-fan-zhixin-miao>
- Amazon:
- <https://www.amazon.com/Modeling-Stability-Analysis-Inverter-Based-Resources-ebook/dp/B0CM8DVJ5G>

# Lingling Fan

**Professor, University of South Florida**

**Dr. Lingling Fan** is Professor at the Department of Electrical Engineering at the University of South Florida. She was with Midwest ISO (St. Paul, Minnesota) from 2001 to 2007. Dr. Fan is research active in control, system identification, and stability analysis of power systems, power electronic converters, and electric machines. Dr. Fan is the founding co-chair of IEEE Power and Energy Society's Wind SSO/IBR SSO task force. She has authored/co-authored three books on dynamic modeling of power grids, synchronous machines, and inverter-based resources. Currently, She serves as the Editor-in-Chief of IEEE Electrification Magazine and Associate Editor for IEEE transactions on Energy Conversion. Dr. Fan was elevated to IEEE Fellow class 2022 for her contributions to stability analysis and control of inverter-based resources and received ESIG Excellence Award in March 2024 for contributions to analysis of power system dynamics and system oscillations in systems with inverter-based resources.

